CrossMark

Abundant Atmospheric Methane from Volcanism on Terrestrial Planets Is Unlikely and Strengthens the Case for Methane as a Biosignature

Nicholas Wogan[1,2] , Joshua Krissansen-Totton[2,3], and David C. Catling[1,2]

[1] Dept. Earth and Space Sciences, University of Washington, Seattle, WA, USA; wogan@uw.edu
[2] Virtual Planetary Laboratory, University of Washington, Seattle, WA, USA
[3] Dept. of Astronomy and Astrophysics, University of California, Santa Cruz, CA, USA

Abstract

The disequilibrium combination of abundant methane and carbon dioxide has been proposed as a promising exoplanet biosignature that is readily detectable with upcoming telescopes such as the James Webb Space Telescope. However, few studies have explored the possibility of nonbiological CH_4 and CO_2 and related contextual clues. Here we investigate whether magmatic volcanic outgassing on terrestrial planets can produce atmospheric CH_4 and CO_2 with a thermodynamic model. Our model suggests that volcanoes are unlikely to produce CH_4 fluxes comparable to biological fluxes. Improbable cases where volcanoes produce biological amounts of CH_4 also produce ample carbon monoxide. We show, using a photochemical model, that high abiotic CH_4 abundances produced by volcanoes would be accompanied by high CO abundances, which could be a detectable false-positive diagnostic. Overall, when considering known mechanisms for generating abiotic CH_4 on terrestrial planets, we conclude that observations of atmospheric CH_4 with CO_2 are difficult to explain without the presence of biology when the CH_4 abundance implies a surface flux comparable to modern Earth's biological CH_4 flux. A small or negligible CO abundance strengthens the CH_4+CO_2 biosignature because life readily consumes atmospheric CO, while reducing volcanic gases likely cause CO to build up in a planet's atmosphere. Furthermore, the difficulty of volcanically generated CH_4-rich atmospheres suitable for an origin of life may favor alternatives such as impact-induced reducing atmospheres.

1. Introduction

Large telescopes will soon be used to search for biogenic waste gases in exoplanet atmospheres. Oxygen is the most extensively studied biosignature gas (Meadows 2017; Meadows et al. 2018). Although many studies have proposed ways of identifying scenarios where nonliving processes might mimic life by producing oxygen (i.e., false positives; Domagal-Goldman et al. 2014; Tian et al. 2014; Wordsworth & Pierrehumbert 2014; Harman et al. 2015; Luger & Barnes 2015; Schwieterman et al. 2019), the circumstances are unusual and contextual clues can distinguish abiotic scenarios (Meadows et al. 2018).

However, even when life is present, oxygen biosignatures may be uncommon. Oxygenic photosynthesis is a complex metabolism that only evolved once on Earth (Fischer et al. 2016). Additionally, oxygen was slow to accumulate in the Earth's atmosphere (Lyons et al. 2014), and other planets may have low O_2 concentrations for billions of years despite having oxygenic photosynthetic life if there are large oxygen sinks (Claire et al. 2006). Accumulation of oxygen may be especially challenging on planets orbiting M-dwarf stars due to their low visible photon flux, which potentially limits primary production (Lehmer et al. 2018).

One alternative to detecting oxygen-rich planets like the modern Earth is to look for methane on planets like the Archean Earth. Before the rise of oxygen, methanogenic life could have sustained a methane-rich atmosphere, which could

be detected with remote spectroscopy (Schindler & Kasting 2000; Kasting & Catling 2003).

Recently, Krissansen-Totton et al. (2018b) proposed a criterion for methane biosignatures: finding abundant CH_4 in the presence of CO_2 (abbreviated CH_4+CO_2). This combination is compelling if the CH_4 mixing ratio is greater than 0.1% because it is difficult to explain such an abundance with the short atmospheric lifetime of CH_4 in terrestrial atmospheres and nonbiological methane sources such as serpentinization (Krissansen-Totton et al. 2018b). This 0.1% threshold value is for planets that orbit stars like the Sun and must be adjusted for different stellar types. For example, planets orbiting M-stars typically receive less near-UV radiation than planets orbiting Sun-like stars, resulting in different photochemistry that promotes the buildup of CH_4 (Segura et al. 2005; Grenfell et al. 2007, 2014; Rugheimer et al. 2015; Rugheimer & Kaltenegger 2018). Krissansen-Totton et al. (2018b) argued that the CH_4 biosignature is strengthened by a low CO abundance because volcanoes that produce CH_4 should also likely generate CO. Additionally, living planets might have low CO because microbes consume CO (Kharecha et al. 2005); coupled ecosystem-planetary models of the early Earth suggest atmospheric CO/CH_4 ratios declined dramatically with the emergence of chemoautotrophic ecosystems (Sauterey et al. 2020).

Exploring false positives for methane biosignatures is timely. Biogenic O_2 or O_3 detections with upcoming telescopes, such as the James Webb Space Telescope (JWST), will be extremely difficult (Barstow & Irwin 2016; Krissansen-Totton et al. 2018a; Fauchez et al. 2019; Lustig-Yaeger et al. 2019; Wunderlich et al. 2020), whereas CH_4+CO_2

biosignatures are more readily detectable. Indeed, an Archean-Earth-like CH_4+CO_2 biosignature is potentially detectable on the planet TRAPPIST-1e, with just 10 transits (Krissansen-Totton et al. 2018a). Thus, exploration of potential methane biosignature false positives and their contextual discriminants is needed.

The literature exploring false positives for methane biosignatures has primarily focused on CH_4 generation in deep-sea serpentinizing hydrothermal vents. Guzmán-Marmolejo et al. (2013) estimated a maximum CH_4 surface flux of 0.18 Tmol yr^{-1} (6.8 × 10^8 molecules cm^{-2} s^{-1}) from hydrothermal vents for planets with the same mass as Earth. Additionally, Krissansen-Totton et al. (2018b) used Monte Carlo simulations to estimate a probability distribution for maximum abiotic CH_4 production from this process. They suggest that >10 Tmol CH4 yr^{-1} is highly unlikely. These estimated maximum fluxes are small compared to modern Earth's biological CH_4 flux of 30 Tmol yr^{-1}.

However, investigations of abiotic CH_4 on Earth suggest that these estimates of abiotic CH_4 from hydrothermal vents are potentially unrealistically large. Serpentinization reactions involving water and ultramafic oceanic crust generate H_2; then, purportedly, H_2 might react with inorganic carbon in hydrothermal systems to generate CH_4. Krissansen-Totton et al. (2018b) and Guzmán-Marmolejo et al. (2013) both estimated abiotic CH_4 fluxes, assuming efficient reactions between H_2 and inorganic carbon. However, laboratory experiments have shown that, uncatalyzed, this reaction is extremely slow at hydrothermal vent temperatures and pressures preventing chemical equilibrium on timescales of at least months (Reeves & Fiebig 2020). Additionally, various lines of evidence suggest that much of the CH_4 observed in deep-sea hydrothermal vent waters is ultimately from biology (Reeves & Fiebig 2020). Furthermore, lifeless planets without silica-secreting organisms should have high ocean-water SiO_2 concentrations, which suppresses the H_2 and therefore abiotic CH_4 produced from serpentinization (Tutolo et al. 2020).

Impacts can likely generate abiotic CH_4 (Zahnle et al. 2020), although impact-generated CH_4 is only probable early in a solar system's lifetime. The cratering record on the Moon shows that Earth's impact flux decreased dramatically by 3.5 Ga (Marchi et al. 2014). Thus, extra-solar systems that are several billion years old are probably unlikely to have abiotic CH_4 from this source.

Here we investigate another potential false-positive for the CH_4+CO_2 biosignature: magma-sourced volcanic outgassing (i.e., not metamorphic). Negligible CH_4 has been observed in gases emitted by magmatic volcanoes on Earth (Catling & Kasting 2017; Reeves & Fiebig 2020), although it has not been investigated whether substantial CH_4 is feasible for volcanoes in vastly different thermodynamic regimes. We simulate outgassing speciation for a range of magma temperatures, outgassing pressures, oxygen fugacities, volatile composition, and variable partitioning between subaerial and submarine volcanism. We examine whether volcanoes can produce CH_4 fluxes comparable to biological fluxes. Using a photochemical model, we also investigate the atmospheric composition of hypothetical planets by reducing volcanic gases to see whether volcanic CH_4 coincides with large atmospheric CO, which could be a detectable false-positive marker.

2. Methods

2.1. Model for Calculating Volcanic Outgassing Speciation

Below, we describe our model for predicting the gases produced by an erupting mantle-sourced volcano. We follow Gaillard & Scaillet (2014) and solve for the gas–gas and gas–melt equilibrium in a C–O–H system. Our model differs from Gaillard & Scaillet (2014) because we do not consider nitrogen or sulfur species. Despite these differences, we obtain similar results to calculations made in Gaillard & Scaillet (2014). We have also validated our code against the work of Liggins et al. (2020) and Ortenzi et al. (2020), which have independently constructed similar outgassing models. Our Python code is published as open-source software on the GitHub page https://github.com/Nicholaswogan/VolcGases.

Figure 1 shows a highly schematic conceptualization of volcanic degassing typical of low-viscosity magma. Gas bubbles form in the magma when molecules like H_2O and CO_2 are exsolved. Within the gas bubbles, reactions drive the system to chemical equilibrium. The oxygen fugacity (f_{O_2}) of the gas bubble is controlled by equilibrium with the oxygen fugacity of the magma (e.g., Kadoya et al. 2020). Gases bubbles are released from the magma and enter the overlying atmosphere or ocean.

A mathematical model describes the volatiles in gas bubbles and magma. The amount of carbon and hydrogen that are exsolved by the magma into bubbles is governed by the solubility of CO_2 and H_2O, which we calculate with the solubility relations for mafic magmas described in Iacono-Marziano et al. (2012):

$$\ln(x_{CO_2}) = x_{H_2O}d_{H_2O} + a_{CO_2}\ln(P_{CO_2}) + S_1, \quad (1)$$
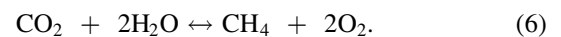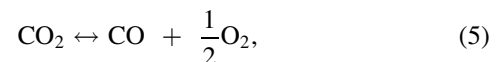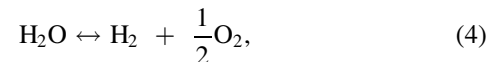
$$\ln(x_{H_2O}) = a_{H_2O}\ln(P_{H_2O}) + S_1. \quad (2)$$

Here x_{CO_2} and x_{H_2O} are mol fractions of CO_2 and H_2O in the magma, respectfully. Additionally, P_{CO_2} and P_{H_2O} are the partial pressure of CO_2 and H_2O in gas bubbles suspended in the magma. The other terms in Equations (1) and (2) are solubility parameters with values shown in Table 1, except S_1 and S_2, which are further described in Appendix A.1. We use solubility relations appropriate for mafic magmas because rocky planets and moons in our solar system usually have basaltic crusts, suggesting that mafic magma is common to most terrestrial bodies.

Volatile mol fractions (e.g., x_{H_2O}) can be converted to mass fractions with the formula

$$m_i = \frac{x_i \mu_i}{\mu_{magma}} \quad (3)$$

Here m_i is the mass fraction, μ_i is the volatile's molar mass, and i can be either H_2O or CO_2. Table 1 gives the units of each term.

We assume that after the hot gas exsolves from the magma into bubbles, it achieves thermodynamic equilibrium from the reactions
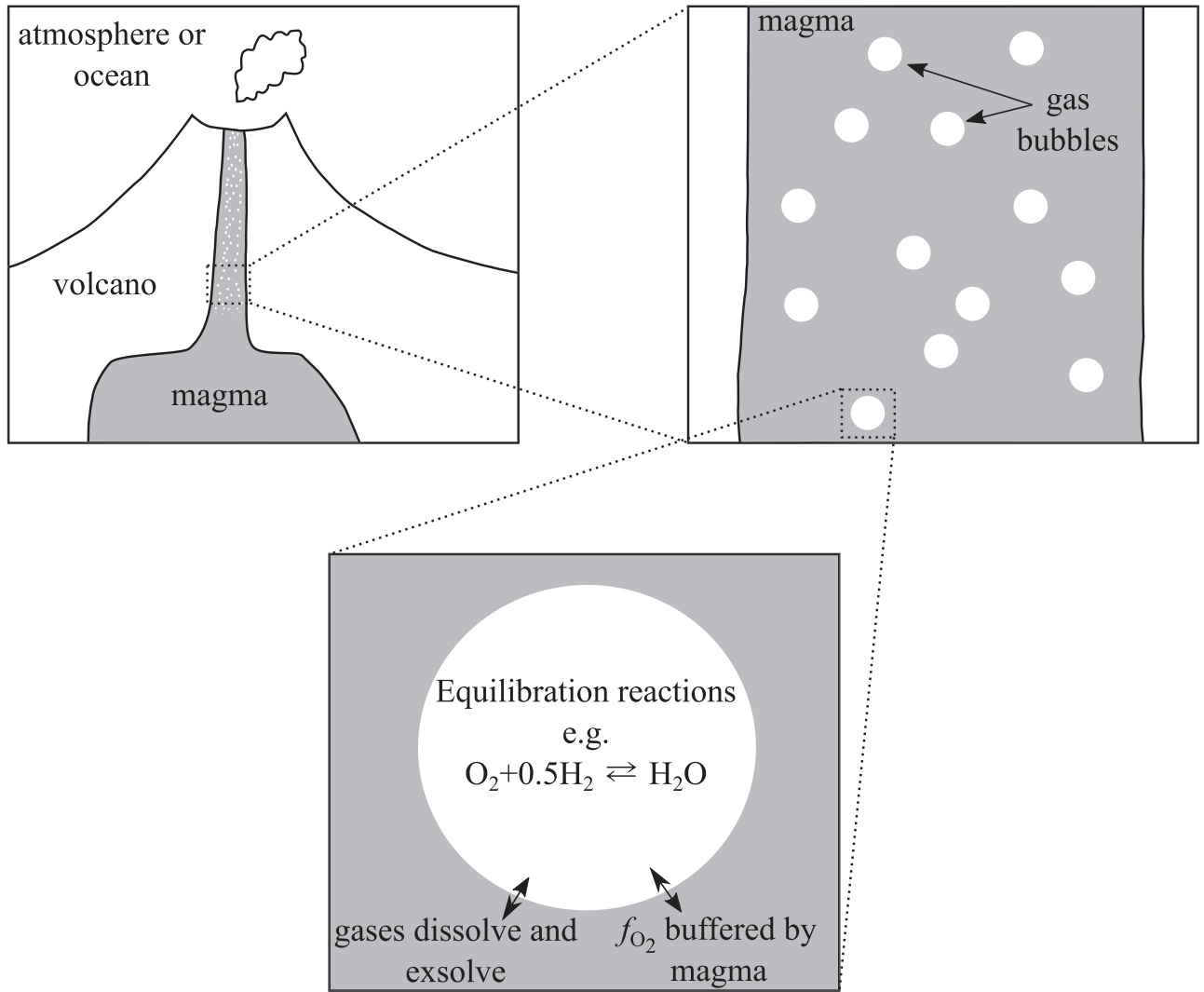
$$H_2O \leftrightarrow H_2 + \frac{1}{2}O_2, \quad (4)$$

$$CO_2 \leftrightarrow CO + \frac{1}{2}O_2, \quad (5)$$

$$CO_2 + 2H_2O \leftrightarrow CH_4 + 2O_2. \quad (6)$$

Figure 1. Qualitative sketch of degassing typical of low-viscosity magma (e.g., Hawaiian volcanoes). Here a gas bubble reaches thermal and chemical equilibrium with a melt (no crystals are present). Note, degassing can occur in many different ways depending on magma viscosity and volatile content (Gonnermann & Manga 2013).

At thermodynamic equilibrium, the ratios of the fugacities of volatile species (denoted f_i) are related to the equilibrium constant corresponding to each chemical reaction. We assume that we can replace fugacities with partial pressures (denoted P_i). This approximation is reasonable for the temperatures and pressures involved in volcanic outgassing (Holland 1984). Thus,

$$K_1 = \frac{f_{H_2} f_{O_2}^{0.5}}{f_{H_2O}} \approx \frac{P_{H_2} f_{O_2}^{0.5}}{P_{H_2O}}, \qquad (7)$$

$$K_2 = \frac{f_{CO} f_{O_2}^{0.5}}{f_{CO_2}} \approx \frac{P_{CO} f_{O_2}^{0.5}}{P_{CO_2}}, \qquad (8)$$

$$K_3 = \frac{f_{CH_4} f_{O_2}^2}{f_{CO_2} f_{H_2O}^2} \approx \frac{P_{CH_4} f_{O_2}^2}{P_{CO_2} P_{H_2O}^2}. \qquad (9)$$

We calculate equilibrium constants (e.g., K_1) using the NASA thermodynamic database (Burcat & Ruscic 2005). We assume that the gas is thermally and chemically coupled to the magma so that the oxygen fugacity (f_{O_2}) of the gas is set by the oxygen

fugacity of magma, as observed (Symonds et al. 1994). So far, we have seven unknowns (x_{CO_2}, x_{H_2O}, P_{CO_2}, P_{H_2O}, P_{CO}, P_{H_2}, P_{CH_4}) and only five equations. To close the system, we add three more equations and one more unknown. The first equation requires that the partial pressures sum to the total pressure:

$$P_{H_2} + P_{H_2O} + P_{CO} + P_{CO_2} + P_{CH_4} = P. \qquad (10)$$

The final two equations are atom conservation equations for carbon and hydrogen:

$$\frac{m_{CO_2}^{tot} \mu_{magma}}{\mu_{CO_2}} = \frac{P_{CO_2} + P_{CO} + P_{CH_4}}{P} \alpha_{gas}$$
$$+ (1 - \alpha_{gas}) x_{CO_2}, \qquad (11)$$

$$\frac{m_{H_2O}^{tot} \mu_{magma}}{\mu_{H_2O}} = \frac{P_{H_2O} + P_{H_2} + 2P_{CH_4}}{P} \alpha_{gas}$$
$$+ (1 - \alpha_{gas}) x_{H_2O}. \qquad (12)$$

Equations (11) and (12) state that the total moles of either carbon or hydrogen should be equal to the moles of either

Table 1
Model Constants and Variables

	Constant or variable	Value	Units	Definition
Constants	d_{H_2O}	2.3	⋯	Solubility constant[a]
	a_{CO_2}	1	⋯	Solubility constant[a]
	a_{H_2O}	0.54	⋯	Solubility constant[a]
	S_1	⋯	⋯	Solubility constant[a]
	S_2	⋯	⋯	Solubility constant[a]
	μ_{magma}	64.52	$\frac{g \; magma}{mol \; magma}$	Molar mass of magma[b]
	μ_{H_2O}	18.02	$\frac{g \; H_2O}{mol \; H_2O}$	Molar mass of H_2O
	μ_{CO_2}	44.01	$\frac{g \; CO_2}{mol \; CO_2}$	Molar mass of CO_2
	K_1	$e^{-29755/T+6.55}$	$bar^{0.5}$	Equilibrium constant[c]
	K_2	$e^{-33979/T+10.42}$	$bar^{0.5}$	Equilibrium constant[c]
	K_3	$e^{-96444/T+0.22}$	⋯	Equilibrium constant[c]
Input	P	⋯	bar	Total pressure of degassing
	T	⋯	K	Temperature of magma and gas
	f_{O_2}	⋯	bar	Oxygen fugacity of the magma
	$m_{CO_2}^{tot}$	⋯	$\frac{g \; CO_2}{g \; gas \; and \; magma}$	Mass fraction CO_2 in magma before degassing
	$m_{H_2O}^{tot}$	⋯	$\frac{g \; H_2O}{g \; gas \; and \; magma}$	Mass fraction H_2O in magma before degassing
Output	x_{H_2O}	⋯	$\frac{mol \; H_2O}{mol \; magma}$	Mol fraction of H_2O in the magma after degassing
	x_{CO_2}	⋯	$\frac{mol \; CO_2}{mol \; magma}$	Mol fraction of CO_2 in the magma after degassing
	P_{H_2O}	⋯	bar	Partial pressure of H_2O
	P_{CO_2}	⋯	bar	Partial pressure of CO_2
	P_{H_2}	⋯	bar	Partial pressure of H_2
	P_{CO}	⋯	bar	Partial pressure of CO
	P_{CH_4}	⋯	bar	Partial pressure of CH_4
	α_{gas}	⋯	$\frac{mol \; gas}{mol \; gas \; and \; magma}$	Mol fraction in gas phase

Notes.
[a] From Iacono-Marziano et al. (2012). See Appendix A.1 to calculate S_1 and S_2.
[b] Molar mass of Mount Etna magma.
[c] Calculated from the NASA thermodynamic database (Burcat & Ruscic 2005).

element in the gas phase plus the moles in the magma. Here α_{gas} is the final unknown. It is the total moles in the gas phase divided by the total moles in the gas and magma combined. See Appendix A.2 for a full derivation of Equations (11) and (12).

Given a gas and magma temperature (T), pressure (P), oxygen fugacity (f_{O_2}), and the total mass fraction (or mol fraction) of CO_2 and H_2O in the magma ($m_{CO_2}^{tot}$, and $m_{H_2O}^{tot}$), Equations (1), (2), (7)–(12) are a system of eight equations and eight unknowns (x_{CO_2}, x_{H_2O}, P_{CO_2}, P_{H_2O}, P_{CO}, P_{H_2}, P_{CH_4}, α_{gas}). We solve this system of equations numerically with the Scipy Python package.

The solution to this system of equilibrium equations provides an estimate of the amount of each volatile species in gas bubbles in magma immediately before the gas leaves the magma. We assume bubbles remain in thermodynamic equilibrium with the surrounding melt until they are released into the overlying atmosphere or ocean, and volatile speciation does not continue to evolve upon release. This does not exactly reflect real degassing. Observed outgassing chemistry suggests that volcanic gas re-equilibrates to temperatures slightly lower than the magma as the gas leaves the magma and is no longer chemically buffered by it (Oppenheimer et al. 2018; Moussallam et al. 2019; Kadoya et al. 2020). We do not capture this complexity in the main text, although in Appendix A.4 we investigate the closed system re-equilibration of volcanic gases and show that this process does not change our conclusions.

Once the unknowns are solved for, they can be used to calculate the gas production (i.e., the moles of gas produced per kilogram of magma erupted):

$$q_i = 10^3 \left(\frac{\alpha_{gas}}{\mu_{magma}(1 - \alpha_{gas})} \right) \frac{P_i}{P}. \tag{13}$$

Here q_i is the gas production of species i in mol gas kg^{-1} magma. Calculating q_i is useful because it is related to the flux F_i of gas i to the atmosphere by the magma production rate:

$$F_i = q_i Q_m. \tag{14}$$

Here Q_m is the magma production rate in kg magma yr^{-1} and F_i is in mol yr^{-1}.

Several authors have shown that degassing can be affected by graphite saturation of magma (Hirschmann & Withers 2008) or by the solubility of CO, CH_4, and H_2 in magma (Hirschmann et al. 2012; Ardia et al. 2013; Wetzel et al. 2013). The gas speciation model described previously does not account for these processes. However, in Appendix A.3, we introduce a more complex model that accounts for graphite saturation and CO, CH_4, and H_2 solubility, and show that this model produces very similar results to the simplified model described here.
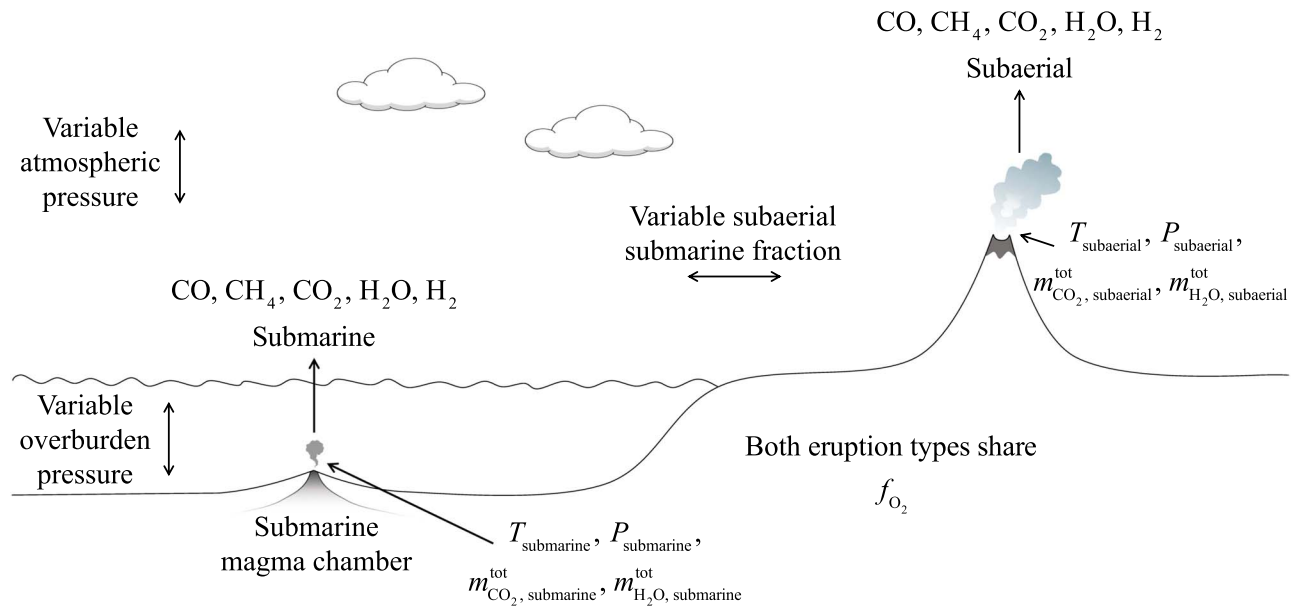
Figure 2. Illustration of the parameters considered in the Monte Carlo simulations.

Table 2
Monte Carlo Sampling Distributions

Variable	Low	High	Sampling method	Justification
$T_{\text{submarine}}$	873 K	1973 K	Linear uniform	Range of submarine magma temperatures observed on Earth[a]
$T_{\text{subaerial}}$	873 K	1973 K	Linear uniform	Range of subaerial magma temperatures observed on Earth[a]
$P_{\text{submarine}}$	100 bar	1000 bar	Linear uniform	Degassing pressure at 1 km to 10 km ocean depth[b]
$P_{\text{subaerial}}$	0.001 bar	100 bar	$\log_{10}$ uniform	Rough range of subaerial degassing pressure in solar system
$m^{\text{tot}}_{\text{CO2, submarine}}$	10^{-5}	10^{-2}	$\log_{10}$ uniform	Approx. CO_2 mass fraction range in Earth magma (Wallace 2005; Wallace et al. 2015; Anderson & Poland 2017; le Voyer et al. 2019)
$m^{\text{tot}}_{\text{CO2,subaerial}}$	10^{-5}	10^{-2}	$\log_{10}$ uniform	Approx. CO_2 mass fraction range in Earth magma (Wallace 2005; Wallace et al. 2015; Anderson & Poland 2017; le Voyer et al. 2019)
$m^{\text{tot}}_{\text{H2O, submarine}}$	10^{-5}	10^{-1}	$\log_{10}$ uniform	H_2O mass fraction range for Earth submarine outgassing (Wallace et al. 2015)
$m^{\text{tot}}_{\text{H2O, subaerial}}$	10^{-5}	10^{-1}	$\log_{10}$ uniform	H_2O mass fraction range for Earth subaerial outgassing (Wallace et al. 2015)
f_{O_2}	FMQ-4	FMQ+5	$\log_{10}$ uniform	Oxygen fugacity of most reducing Martian meteorite (Catling & Kasting 2017) to most oxidized magma on Earth (Stamper et al. 2014)[c]
X	0	1	Linear uniform	0% to 100% subaerial volcanism

Notes.
[a] Coldest rhyolite magma and hottest komatiites magmas (Huppert et al. 1984).
[b] Assumes Earth's gravity. The solubility of H_2O in magma does not allow for significant CH_4 degassing at pressures greater than 1000 bar, equivalent to a depth of 10 km.
[c] FMQ is the fayalite-magnetite-quartz mineral redox buffer. See Chapter 7 in Catling & Kasting (2017) for a description of mineral redox buffers. We use the parameterization for the FMQ buffer defined by Wones & Gilbert (1969). This parameterization has only been experimentally validated to 1400 K (O'Neill 1987), but we extrapolate using the parameterization to 1973 K.

2.2. Monte Carlo Simulations

We investigate volcanic false positives to the CH_4+CO_2 biosignature on two types of worlds: an Earth-like world with subaerial and submarine outgassing (Figure 2) and an ocean world with only submarine outgassing. For each type of planet, we search for false-positive scenarios by calculating volcanic outgassing speciation with a wide range of input parameters.

To explore volcanism on Earth-like planets, we calculate outgassing speciation 10,000 times. For each calculation, we sample either uniform or $\log_{10}$-uniform distributions (see Table 2) of 10 parameters: $T_{\text{submarine}}$, $P_{\text{submarine}}$, $m^{\text{tot}}_{\text{CO2, submarine}}$, $m^{\text{tot}}_{\text{H2O, submarine}}$, $T_{\text{subaerial}}$, $P_{\text{subaerial}}$, $m^{\text{tot}}_{\text{CO2, subaerial}}$, $m^{\text{tot}}_{\text{H2O, subaerial}}$, f_{O_2}, and X. The width of each uniform sampling distribution is given and explained in Table 2. We use inputs

with subscripts "subaerial" to calculate subaerial volcanic speciation and inputs with subscripts "submarine" to calculate submarine volcanic speciation, and then we combine the results of each calculation with the formula

$$n_i = \frac{P_{i,\text{ subaerial}}}{P_{\text{subaerial}}}X + \frac{P_{i,\text{ submarine}}}{P_{\text{submarine}}}(1-X). \qquad (15)$$

Here n_i is the mixing ratio of averaged outgassed volatiles of species i produced by the combination of subaerial and submarine volcanoes and X is the fraction of subaerial volcanism ($0 < X < 1$). Also, $P_{i,\text{subaerial}}$ and $P_{i,\text{submarine}}$ are the partial pressure of species i in subaerial and submarine outgassing, respectively.
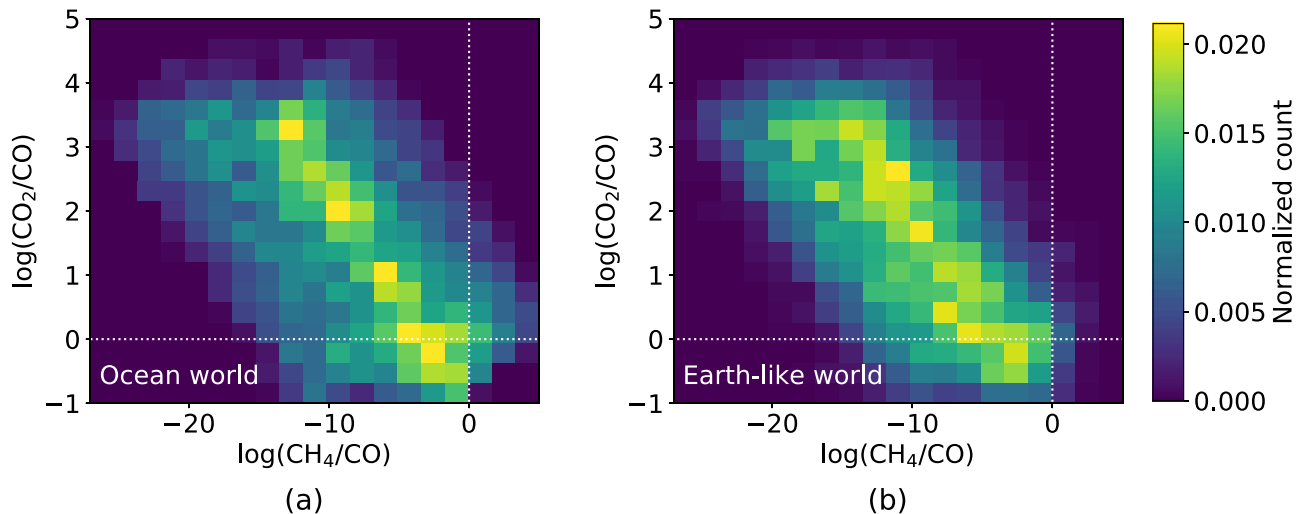
Figure 3. Results of the Monte Carlo simulation described in Section 2.2. (a) and (b) show normalized count as a function of $\log(CH_4/CO)$ and $\log(CO_2/CO)$ for an ocean world and Earth-like world, respectively. The white dotted lines indicate where $CH_4/CO = 1$ and $CO_2/CO = 1$. For almost all calculated gas speciations, CO_2 and CO are much more abundant than CH_4.

To investigate volcanism on an ocean world, we also calculate outgassing speciation 10,000 times. For each calculation, we sample either uniform or $\log_{10}$-uniform distributions of inputs $T_{\text{submarine}}$, $P_{\text{submarine}}$, $m^{\text{tot}}_{CO_2,\text{ submarine}}$, $m^{\text{tot}}_{H_2O,\text{ submarine}}$, and f_{O_2}, with ranges defined and justified in Table 2.

2.3. Photochemical Modeling: Uninhabited Anoxic Ocean World with Reducing Volcanic Gases

We further investigate the CH_4+CO_2 biosignature by modeling the atmospheric composition of hypothetical uninhabited ocean worlds with reducing volcanic gases. We consider planets orbiting the Sun and a late M star—the latter because planets orbiting M-dwarfs are the most feasible targets for near-term telescopes like JWST (Barstow & Irwin 2016). Additionally, we simulate ocean worlds because ocean-bottom degassing is most thermodynamically prone to produce CH_4, as revealed by our Monte Carlo simulations and previous studies (French 1966; Kasting & Brown 1998; see Section 4.1.1 for further discussion).

To simulate atmospheres on uninhabited planets, we use the 1-D photochemical model contained within the open-source software package *Atmos*. *Atmos* is derived from a model originally developed by the Kasting group (Pavlov et al. 2001), and versions of this code have been used to simulate the Archean and Proterozoic Earth atmosphere (Zahnle et al. 2006), Mars (Zahnle et al. 2008; Smith et al. 2014; Sholes et al. 2019), and exoplanet atmospheres (Harman et al. 2015; Schwieterman et al. 2019).

3. Results

3.1. Monte Carlo Simulations

Figure 3 shows joint distributions of gas ratios CH_4/CO and CO_2/CO from the Monte Carlo simulation described in Section 2.2. These results suggest that for most combinations of parameters, volcanoes are most likely to produce more CO_2 than CO, and negligible CH_4, which is the case for the modern Earth (Catling & Kasting 2017). About 7% and 2% of calculations produce more CH_4 than CO for ocean worlds and Earth-like worlds, respectfully. In the vast majority of cases, either CO or CO_2 is the dominant carbon-bearing species.

Figures 4(a) and (b) show CH_4 production from the Monte Carlo simulations in terms of mol CH_4 kg^{-1} magma. To give a sense of the gas fluxes implied by these CH_4 productions, we multiply the distributions in Figures 4(a) and (b) by the magma production rate of modern Earth of 9×10^{13} kg yr^{-1} (Crisp 1984), which gives the gas fluxes shown in Figures 4(c) and (d), respectively. About 0.1% of calculations predict more than 10 Tmol CH_4 yr^{-1} for both Earth-like worlds and ocean worlds. This small fraction suggests that for modern Earth magma production rates, volcanoes are unlikely to produce CH_4 fluxes comparable to modern Earth's biological flux of 30 Tmol yr^{-1} (Hauglustaine et al. 2007).

Magma production rates larger than modern Earth's increase the probability that volcanic fluxes of CH_4 become comparable to biological CH_4 fluxes. For example, the early Archean Earth could have had magma production rates up to about 25 times modern Earth's (Sleep & Zahnle 2001). Such a magma production rate would shift the distributions in Figures 4(c) and (d) to larger values by a factor of 25 (or in $\log_{10}$-space, by a factor of 1.4). In this case, ~2% of calculations (for either Earth-like world or ocean world) would predict more than 10 Tmol CH_4 yr^{-1}.

Crucially, large CH_4 fluxes should almost always coincide with even larger CO fluxes (horizontal axis in Figure 3). Therefore, the unlikely cases where volcanoes mimic biological CH_4 fluxes can be identified by detecting abundant CO in a planet's atmosphere. We further investigate CO as a CH_4+CO_2 biosignature discriminant using a photochemical model in the following section.

3.2. Photochemical Modeling: Uninhabited Anoxic Ocean World with Reducing Volcanic Gases

We use the *Atmos* photochemical model to simulate the potential observable gas abundances of uninhabited Earth-sized ocean worlds with reducing volcanic gases. We consider such planets because they are the most prone to mimic biology by producing volcanic CH_4 (see Section 4.1.1 for more details). Our hypothetical planets have 1 bar N_2 dominated atmospheres, 400 bars of ocean water, magma degassing at 1473 K, and mantle redox states of FMQ-4. Here FMQ is the
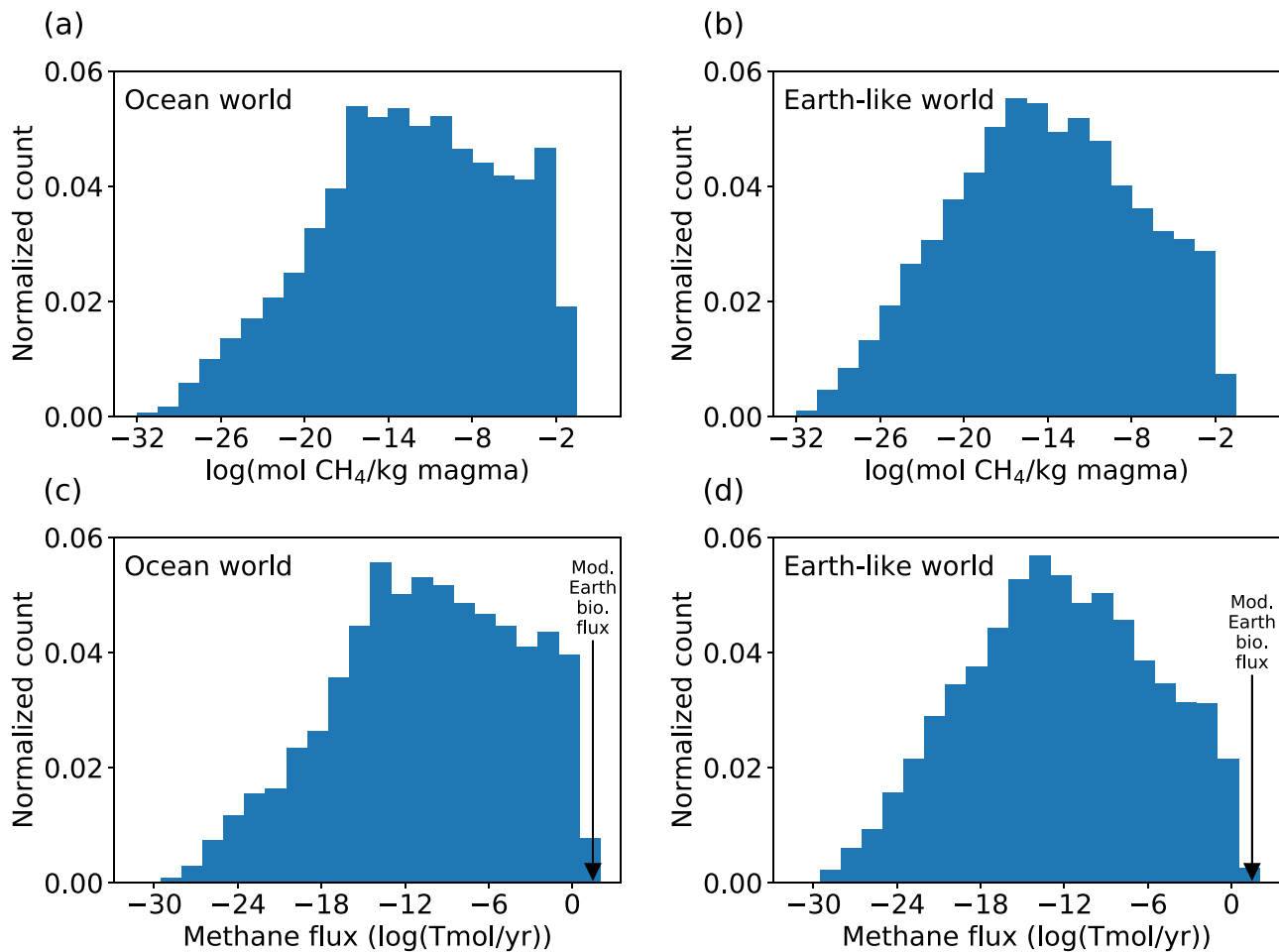
Figure 4. Normalized count of methane production (mol gas/kg magma) for (a) ocean worlds and (b) Earth-like worlds. Distributions were calculated by sampling the ranges in Table 2. Multiplying Earth's magma production rate of 9×10^{13} kg magma yr^{-1} by (a) and (b) gives the methane fluxes in (c) and (d), respectively. For modern Earth's magma production rate, volcanoes are likely to produce negligible CH_4.

fayalite-magnetite-quartz buffer, which is a synthetic reference f_{O_2} value at fixed temperature-pressure conditions. Additionally, we assume that the magma contains 0.1 wt% CO_2 and 1 wt% H_2O. Our assumed H_2O concentration is comparable to those observed in submarine hot-spot magmas (0.2 to 1.5 wt%; Wallace et al. 2015); however, the CO_2 concentration we assume is slightly lower (Anderson & Poland 2017). Given these inputs, our speciation model (Section 2.1) predicts gas production from erupted magma of $q_{H_2} = 4.36 \times 10^{-2}$ mol gas/kg magma, $q_{CO} = 1.29 \times 10^{-2}$ mol gas/kg magma, and $q_{CH_4} = 7.39 \times 10^{-3}$ mol gas/kg magma.

The magnitude of gas fluxes to the atmosphere resulting from chemically reducing volcanism depends on the magma production rate (Equation (14)). We consider magma production rates between about 10^{-3} and 10^2 Earth's modern magma production rate of 9×10^{13} kg magma yr^{-1} (Crisp 1984).

For each magma production rate, we calculate the outgassing flux of CH_4, H_2, and CO and set these fluxes as lower boundary conditions to the *Atmos* photochemical model. (The outgassing model also gives CO_2 and H_2O fluxes, but we do not use them in our photochemical modeling.) *Atmos* only allows fixed CO_2 mixing ratios and not CO_2 fluxes, so we consider cases with low and high CO_2 (100 ppm and 10%). Additionally, we set the deposition velocity of CO to 10^{-8} cm s^{-2} to reflect the abiotic uptake of CO by the ocean (Kharecha et al. 2005). All other

boundary conditions are specified in Appendix B. Given volcanic outgassing fluxes and other boundary conditions, *Atmos* calculates the mixing ratios of all species when the atmosphere is at photochemical equilibrium.

Figure 5 shows the photochemical modeling results of reducing volcanic gases on an uninhabited Earth-sized ocean world orbiting the Sun. Figure 5(a) assumes that the atmosphere has 100 ppmv CO_2, while Figure 5(b) assumes that atmospheric CO_2 is 10%. Carbon monoxide and methane are more abundant in the model with more CO_2 because CO_2 shields the lower atmosphere from hydoxyl (OH) production from water photolysis. In anoxic atmospheres, OH is a significant sink for both CO and CH_4 through the reactions $CO_2 + OH \rightarrow CO_2 + H$ and $CH_4 + OH \rightarrow CH_3 + H_2O$. OH is generated primarily from H_2O photolysis ($H_2O + h\nu [\lambda < 200$ nm$] \rightarrow OH + H$), but CO_2 shields H_2O from photolysis in model runs with 10% CO_2, thus limiting the CH_4 and CO destruction from OH. Also, CH_4 is more abundant in atmospheres with more CO_2 because CO_2 shields CH_4 from direct photolysis in cases when CO_2 is >200 times as abundant as CH_4. This factor of ~200 comes from comparing Lyα ($\lambda = 121.6$ nm) CO_2 and CH_4 cross sections. Lyα is the portion of the UV spectrum primarily responsible for photolyzing CH_4.

Figure 5 suggests that reducing volcanic gases on an ocean world orbiting a Sun-like star will only mimic biological CH_4
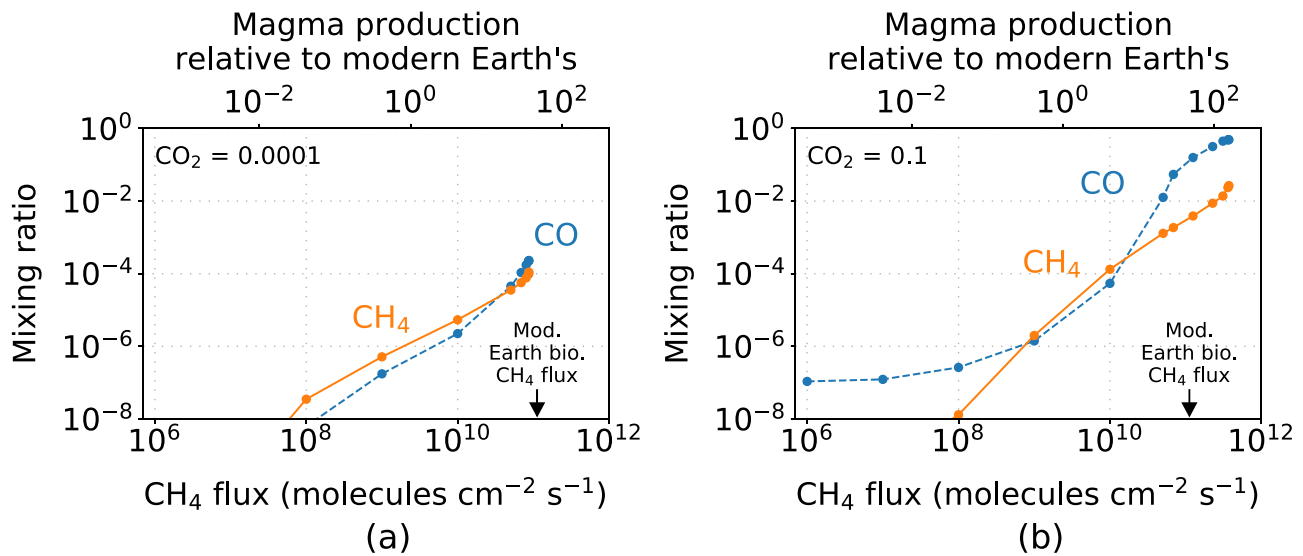
Figure 5. Atmospheric mixing ratios of CO and CH_4 as a function of magma production rate relative to modern Earth's (or CH_4 flux) on an anoxic ocean world with reducing volcanic gases orbiting a Sun-like star. (a) and (b) are identical model runs, except (a) assumes a constant atmospheric CO_2 mixing ratio of 0.0001, and (b) assumes a constant atmospheric CO_2 mixing ratio of 0.1. Modern Earth's biological CH_4 flux is indicated on the horizontal axes. Archean Earth-like CH_4 fluxes and abundances are only mimicked by volcanoes for magma production rates >10 times modern Earth's. Such false-positive cases can be distinguished from biology because the CO abundance exceeds the CH_4 abundance, which would likely not be the case for an inhabited planet.
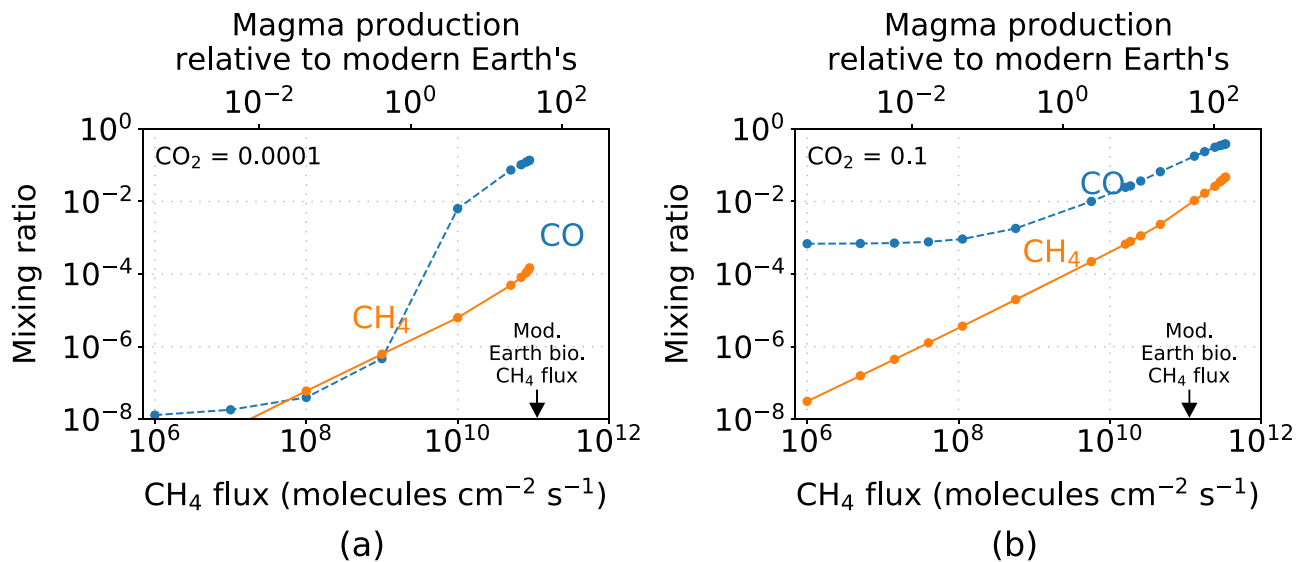

Figure 6. Identical to Figure 5, except for a planet that orbits an M8V star instead of a Sun-like star.

fluxes and abundances for large magma production rates. Volcanism can generate Earth's modern biological CH_4 flux when the magma production rate is ∼50 times modern Earth's (Figure 5). In this case, the photochemical model predicts an atmospheric CH_4 abundance between 0.01% and 0.3%, depending on the CO_2 mixing ratio. Such CH_4 abundances are similar to the 0.01% to 1% expected in the early Archean Earth atmosphere (Catling & Zahnle 2020). In contrast, magma production rates comparable to the modern Earth's result in a CH_4 flux of 2.4×10^9 molecules cm^{-2} s^{-1} (0.64 Tmol yr^{-1}) and CH_4 abundances <30 ppm, which are likely to be considered abiotic levels in an anoxic atmosphere.

Figure 6 shows the CO and CH_4 mixing ratios on an Earth-sized ocean world with reducing volcanic gases orbiting a cold M star. CO and CH_4 are more abundant on the ocean world orbiting the M star compared to the ocean world orbiting a Sun-like star (Figure 5). This is because M8V stars have a low flux of

near-ultraviolet radiation compared to Sun-like stars. The low near-ultraviolet flux reduces OH produce from H_2O photolysis, thus allowing for relatively high CO and CH_4 concentrations.

One consequence of M-dwarf photochemistry is a higher likelihood of Archean Earth-like CH_4 abundances on uninhabited planets with reducing gases from volcanism. Figure 6 shows that modern Earth magma production rates can result in CH_4 abundances up to 0.01%, which is comparable to what is expected in the Archean atmosphere.

Potential CH_4 biosignature false positives from reducing volcanic gases might be discriminated from inhabited worlds using observations of CO. For planets orbiting Sun-like stars (Figure 5) or M stars (Figure 6), the CO abundance is higher than the CH_4 abundance in every case that is a potential outgassing false-positive. Some authors have argued that a large CO abundance is unlikely on an inhabited planet, because atmospheric CO should be readily consumed by biology
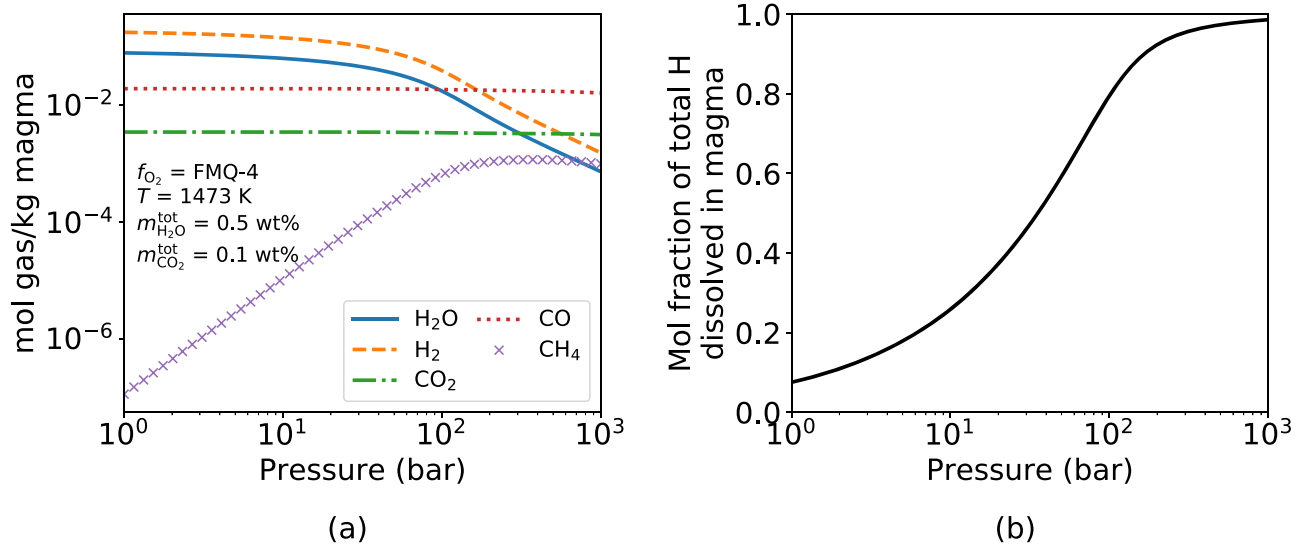
Figure 7. (a) Modeled gas speciation as a function of pressure. (b) Mole fraction of total hydrogen dissolved in the magma as a function of pressure. Model assumes f_{O_2} = FMQ-4, T = 1473 K, $m_{H_2O}^{tot}$ = 0.5 wt%, and $m_{CO_2}^{tot}$ = 0.1 wt%. Methane becomes more prevalent in volcanic gases at higher pressures but asymptotes because hydrogen dissolves into the magma, reducing the total amount of H-bearing volatiles released from the magma.

(Krissansen-Totton et al. 2018a). Conversely, Schwieterman et al. (2019) has demonstrated hypothetical cases where large CO can coincide with biology in an anoxic atmosphere. We further discuss CO as a false-positive discriminant in Section 4.2.

4. Discussion

4.1. The Reasons Why Volcanoes Produce Little CH₄

Our modeling results show that for modern Earth magma production rates, volcanic fluxes of reducing gases are unlikely to produce more than 1 Tmol CH₄ yr⁻¹, even in an extreme case (Figure 4). This flux is relatively small compared to the flux of other volcanic gases on modern Earth. For example, Earth's modern volcanoes produce about 7.5 Tmol CO₂ yr⁻¹ and 95 Tmol H₂O yr⁻¹ (Catling & Kasting 2017, p. 203). There are three main reasons why the outgassing model predicts little CH₄, which we explore further in the following discussion.

4.1.1. Volcanoes Produce Little CH₄ because of Water Solubility in Magma

One reason for small CH₄ outgassing is the high solubility of water in magma at high pressures. Consider Equation (9), which can be re-arranged as follows:

$$\frac{P_{CH_4}}{P_{CO_2}} = \frac{K_3 P_{H_2O}^2}{f_{O_2}^2}. \tag{16}$$

The ratio P_{CH_4}/P_{CO_2} in a gas bubble in magma is directly proportional to $P_{H_2O}^2$ within that bubble. Generally speaking, P_{H_2O} increases as the total pressure of degassing increases because all partial pressures must sum to the total pressure (Equation (10)). For example, subaerial degassing at ∼1 bar will have a relatively small P_{H_2O} and thus a small P_{CH_4}/P_{CO_2} ratio. On the other hand, submarine degassing at ∼400 bar should have a larger H₂O partial pressure and thus a larger P_{CH_4}/P_{CO_2} ratio. Here the equilibrium constant and oxygen fugacity have extremely weak pressure dependencies (i.e., they are effectively constant as degassing pressure changes).

Figure 7(a) shows modeled gas speciation for highly reducing volcanism (f_{O_2} = FMQ-4) as a function of pressure. For small pressures (<100 bar), CH₄ increases with increasing pressure and then asymptotes for pressures >100 bar.

CH₄ asymptotes because of the high solubility of water in magma at high pressure. High pressures dissolve a large fraction of the total available hydrogen as H₂O into the magma, which is shown in Figure 7(b). Dissolving a large amount of H₂O into the magma limits the amount of hydrogen available in the gas phase for making H-bearing species, like CH₄, H₂O, and H₂.

In summary, high pressure is in some ways thermodynamically favorable for making methane because $P_{CH_4} / P_{CO_2} \propto P_{H_2O}^2$, but it is also unfavorable because high pressure dissolves a large fraction of the available hydrogen in the magma as H₂O. Limited amounts of hydrogen in gas bubbles result in small amounts of CH₄ produced.

Kasting & Brown (1998) used Equation (16) to argue that ∼1% of the carbon outgassed by submarine volcanoes should be CH₄ for magma with f_{O_2} = FMQ. They assumed that $P_{H_2O} \approx P$, the total pressure. This assumption is valid for oxidized subaerial volcanoes because ∼90% of the gas exsolved by Earth's subaerial volcanoes is H₂O (Catling & Kasting 2017, p. 203). However, $P_{H_2O} < P$ for submarine volcanoes because of the high-water solubility in magma at high pressure. Our outgassing model, which accounts for water's solubility in magma, produces negligible methane.

Li & Lee (2004) also predict abundant CH₄ produced by subaerial and submarine volcanoes (their Figure 5). However, they calculated equilibrium constants in units of bars and then used units of Pascals for equilibrium chemistry calculations. The result was that they calculated speciation for pressures a factor 10,000 times greater than reported. For example, we were able to reproduce their subaerial outgassing case (their Figure 5(a)) by assuming P = 10,000 bar and not the P = 1 bar total pressure they intended. Additionally, like Kasting & Brown (1998), they did not account for the high solubility of H₂O in magma at high pressure. Their methods assume the total hydrogen outgassed for submarine volcanoes is the same as the total hydrogen outgassed by subaerial volcanoes. This should not be the case, because at
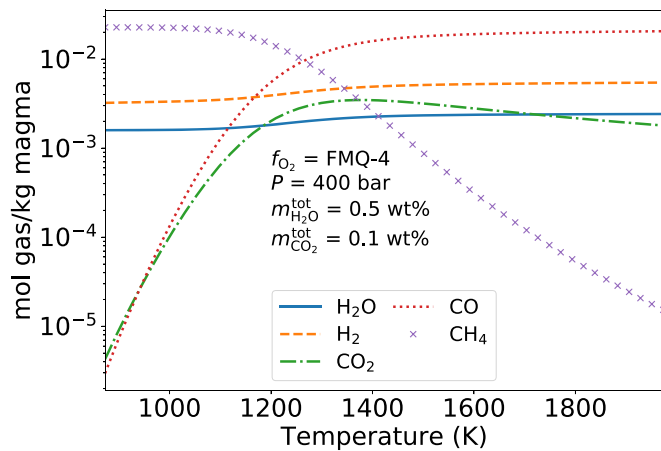
Figure 8. Modeled volcanic outgassing speciation as a function of temperature. Model assumes f_{O_2} = FMQ-4, P = 400 bar, $m_{H_2O}^{tot}$ = 0.5 wt%, and $m_{CO_2}^{tot}$ = 0.1 wt%. CH$_4$ is more thermodynamically favorable at lower degassing temperatures.

Figure 9. Modeled volcanic outgassing speciation as a function of oxygen fugacity. Model assumes P = 400 bar, T = 1473 K, $m_{H_2O}^{tot}$ = 0.5 wt%, and $m_{CO_2}^{tot}$ = 0.1 wt%. Methane is most favorable at low oxygen fugacity.

high pressure water dissolves in magma and is unavailable for making H-bearing gas species (Figure 7(b)).

The pressure dependence of volcanic outgassing has implications for planetary atmospheres generally (Gaillard & Scaillet 2014). Thin atmospheres will allow substantial degassing of both carbon and hydrogen bearing species. However, planets with thick atmospheres or large global oceans will have volcanic degassing dominated by CO_2 and CO, and almost no hydrogen bearing species. The overburden pressure where C-bearing species dominate depends primarily on the un-degassed concentrations of H_2O and CO_2 in the magma. In Figure 7, CO_2 and CO overwhelm H-bearing species at ∼1000 bar for initial volatile concentrations of $m_{CO_2}^{tot}$ = 0.1% and $m_{H_2O}^{tot}$ = 0.5%. In contrast, Figure 8 in Gaillard & Scaillet (2014) illustrates a case with less volatiles ($m_{CO_2}^{tot}$ = 0.007% and $m_{H_2O}^{tot}$ = 0.03%) where C-bearing species eclipse H-bearing species at ∼1 bar.

4.1.2. Volcanoes Produce Little CH$_4$ because Magma Is Hot

Relatively little CH$_4$ is produced by volcanoes because CH$_4$ is generally not thermodynamically favorable at typical magma degassing temperatures. Figure 8 shows gas speciation as a function of temperature for a submarine outgassing case. For these chosen inputs, CH$_4$ is the dominant carbon-bearing species for T < 1200 K. Mid-ocean ridge basalts (MORB) are about 2/3 of total magma produced on Earth (Crisp 1984). MORB magma erupts at temperatures between 1473 and 1650 K (Scheidegger 1973) and are thus in a temperature regime where CH$_4$ is unfavorable, even from more reducing volcanism.

On the other hand, magma from arc volcanoes is generally much colder than MORB magma. Moussallam et al. (2019) report magma temperatures for many arc volcanoes (their Table S3), the coldest of which are 1123 K. Thus, it does seem possible for magma to be cold enough for CH$_4$ to be the dominant carbon-bearing outgassed species from an extremely reducing volcano with f_{O_2} = FMQ-4.

Recall that large magma production rates (∼30x modern) are required for volcanoes to produce CH$_4$ fluxes compared to biological ones (Figure 5). It seems unlikely that planets with large magma production rates will have magma temperatures cold enough to produce plentiful CH$_4$. For example, the Archean Earth may have had a larger magma production rate than the
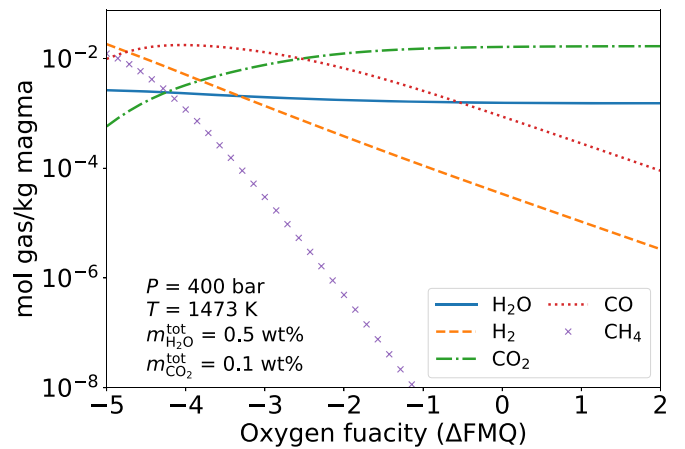
modern Earth because the Earth's mantle was hotter in the distant past (Sleep & Zahnle 2001). The hotter Archean mantle resulted in the eruption of ∼1800 K komatiite magmas (Huppert et al. 1984) or possibly only ∼1600 K (McKenzie 2020). Such hot magma degassing is unfavorable for methane (Figure 8).

4.1.3. Volcanoes Produce Little CH$_4$ because Very Low Oxygen Fugacity Is Required

The final reason why volcanic CH$_4$ is unlikely on terrestrial planets is because very low f_{O_2} is required to make abundant methane. Figure 9 shows gas speciation as a function of oxygen fugacity for submarine volcanism. For these assumed inputs, methane is a substantial fraction of outgassed species for f_{O_2} < FMQ-3, and at FMQ-5 (roughly equivalent to the quartz-fayalite-iron buffer), half the carbon is converted to CH$_4$, while the other half is CO. Most degassing on Earth occurs at approximately f_{O_2} = FMQ (Catling & Kasting 2017, p. 208), but magma spans FMQ-4 to FMQ+5 (Stamper et al. 2014). Additionally, the oxygen fugacity of Martian meteorites ranges between FMQ and FMQ-3.7 (Catling & Kasting 2017, p. 363). Therefore, the f_{O_2} < FMQ-3 required for plentiful CH$_4$ outgassing is at the extremes of the oxygen fugacities observed for Earth and Mars.

Astronomical observations and geochemical experiments suggest Earth-sized planets should generally have relatively oxidized magmas. Doyle et al. (2019) spectroscopically measured the oxygen fugacity of material polluting the surface of several white dwarfs. Their observations suggest that rocky exoplanets are likely to have similar oxygen fugacities to Earth and Mars. Additionally, high pressure experiments suggest that the upper mantles of Earth-sized planets should self-oxidize by iron oxide disproportionation to roughly FMQ during the magma-ocean phase, early in a planet's life (Armstrong et al. 2019).

4.2. Carbon Monoxide as a Methane Biosignature Discriminant

CO-consuming life evolved very early on Earth (Adam et al. 2018) and is a relatively simple metabolism. Therefore, it seems possible that life on other planets will evolve to consume CO. Planets with atmospheric CH$_4$+CO_2 produced by life might also have relatively small amounts of atmospheric CO because of CO

consumers. Consequentially, the presence of abundant CO along with CH_4 can discriminate abiotic situations.

Monte Carlo simulations show that volcanoes should almost always produce more CO than CH_4 (Figure 3). Additionally, photochemical modeling (Figures 5 and 6) suggests that CO should build up in the atmospheres of uninhabited planets with reducing submarine volcanic gases. Thus atmospheric CO_2+CH_4 produced by volcanoes is likely accompanied by a large CO concentration. This is distinct from an inhabited world, which can have lower CO concentrations due to CO-consuming life.

However, the mere presence of large atmospheric CO is not a definitive sign of an uninhabited planet with reducing volcanic gases (Schwieterman et al. 2019). This is because there are limits to how quickly gases can be transported from the atmosphere into the ocean where they can be consumed by life (Kharecha et al. 2005). For example, consider a planet with a very large volcanic CO flux (e.g., 100x modern). CO could build up in this planet's atmosphere even if CO consumers were present in an ocean because CO transport from the atmosphere to the ocean would not be sufficient to maintain low atmospheric CO.

In summary, the CH_4+CO_2 biosignature is most compelling when the CO abundance is low or negligible because a lack of CO potentially implies the presence of CO-consuming biology. In comparison, atmospheric CH_4+CO_2 and large CO is ambiguous, and can either be explained by reducing volcanic gases or by an inhabited world that is unable to sequester atmospheric CO.

JWST might be able to put a tentative upper limit on atmospheric CO. Krissansen-Totton et al. (2018a) simulated JWST retrievals of TRAPPIST-1e with an atmospheric composition similar to the Archean Earth containing 10 ppbv CO. Their synthetic retrieval suggested CO was below 652 ppmv with 90% confidence after 10 transits. CO constraints could be improved by co-adding more transits and positive CO detections may also be possible with JWST (Wunderlich et al. 2020).

However, even if observational CO constraints are poor, it may still be possible to say something about the abiotic or biotic origin of atmospheric CH_4. Reducing gases from volcanism is unlikely to mimic the modern biological CH_4 flux of 30 $Tmol\,yr^{-1}$ (Section 4.1). Additionally, serpentinization is unlikely to produce 30 $Tmol\ CH_4\,yr^{-1}$, and impact-generated CH_4 might be distinguished with system age (Krissansen-Totton et al. 2018b). Therefore, JWST observations of atmospheric CH_4+CO_2 would be challenging to explain without the presence of biology regardless of atmospheric CO, as long as the CH_4 abundance implies a surface flux similar to the modern Earth's.

4.3. CH₄ Levels and Implications for the Origin on Life

Much current origin of life research revolves around the "RNA world" hypothesis (Gilbert 1986; Joyce & Szostak 2018; Sasselov et al. 2020). This hypothesis proposes an interval of time when primitive life consisted of self-replicating, evolving RNA molecules, which, at some point, were encapsulated in cells. On a rocky world, "RNA world" requires that RNA is synthesized from early raw materials. Laboratory experiments that have successfully synthesized nucleobases, which are building blocks of RNA, require the following nitriles: hydrogen cyanide (HCN), cyanoacetylene (HCCCN), and cyanogen (NCCN; Sutherland 2016; Ritson et al. 2018; Benner et al. 2019). In addition, nitriles have

also been used to synthesize amino acids (Miller & Urey 1959; Sutherland 2016).

The known natural source of nitriles is photochemistry in a chemically reducing atmosphere containing H_2, CH_4 and N_2 or perhaps NH_3. For example, Titan's photochemistry produces all the aforementioned nitriles (Strobel et al. 2009). Importantly, to make the simplest nitrile, HCN, requires abundant CH_4 because HCN is formed from photochemical products of CH_4 and nitrogen (Zahnle 1986; Tian et al. 2011).

Our results show that volcanic gases generally are unlikely to cause high atmospheric CH_4 abundances in prebiotic atmospheres. Consequently, the results lend credence to alternative proposals for creating early CH_4-rich, reducing atmospheres, such as impacts (Zahnle et al. 2020). Impacts can create a reducing atmosphere when reactions between iron-rich impact ejecta and shock-heated water vapor from an ocean generate copious H_2, CH_4, and NH_3. Subsequent photochemistry would generate HCN and other prebiotic nitriles over thousands to millions of years (Zahnle et al. 2020).

5. Conclusions

Our modeling of volcanic outgassing speciation suggests that chemically reducing volcanism on terrestrial planets is unlikely to mimic biological CH_4 fluxes. The improbable cases where volcanoes do produce biological CH_4 fluxes also often produce CO. Volcanoes are not prone to produce CH_4 for several reasons. First, the high solubility of H_2O in magma limits the amount of total hydrogen outgassed, thus preventing the production of H-bearing molecules like CH_4. Second, CH_4 outgassing requires relatively low magma temperatures compared to the majority of magma erupted on Earth. Finally, CH_4 outgassing requires a very low magma oxygen fugacity, unlike that of most terrestrial planets inferred from astronomical data (Doyle et al. 2019).

We use a photochemical model to calculate the atmospheric composition of planets with volcanoes that produce CH_4. We find that atmospheric CH_4 should coincide with abundant CO. On the other hand, biogenic CH_4 can coincide with a low CO abundance if CO-consuming microbial life is present.

Therefore, the CH_4–CO_2 biosignature is most compelling when little or no atmospheric CO is detected. Atmospheric CH_4-CO_2 and large CO is ambiguous and can be explained by an uninhabited planet with highly reducing volcanic gases, or an inhabited planet where biology is unable to sequester atmospheric CO (Schwieterman et al. 2019).

However, observations of CO are not required to make conclusions about the abiotic or biotic origin of observed atmospheric CH_4. Atmospheric CH_4 and CO_2 alone would have a reasonable probability of being biological if the observed CH_4 abundance implies a surface flux similar to modern Earth's biological CH_4 flux (30 $Tmol\,yr^{-1}$). Such a large CH_4 flux is difficult to explain with reducing volcanic gases or other abiotic processes that generate CH_4, such as serpentinization.

These conclusions should be taken with caution because they are based on what is understood about processes occurring on the Earth and our Solar System, which may be a very sparse sampling of what is possible.

Table 3
Mount Etna Magma Composition

Magma component	Mole fraction
x_{SiO_2}	0.516
x_{TiO_2}	0.014
$x_{Al_2O_3}$	0.110
x_{FeO}	0.091
x_{MgO}	0.092
x_{CaO}	0.126
x_{Na2O}	0.035
x_{K_2O}	0.002
$x_{P_2O_5}$	0.016

Note. Taken from Iacono-Marziano et al. (2012).

$$\left[\frac{\text{NBO}}{\text{O}}\right]$$
$$= \frac{2(x_{K_2O} + x_{Na_2O} + x_{CaO} + x_{MgO} + x_{FeO} - x_{Al_2O_3})}{2x_{SiO_2} + 2x_{TiO_2} + 3x_{Al_2O_3} + x_{MgO} + x_{FeO} + x_{CaO} + x_{Na_2O} + x_{K_2O}}. \quad \text{(A3)}$$

Appendix A
Details of Outgassing Speciation Model

A.1. Solubility Constants for H₂O and CO₂

Our outgassing model uses solubility equations for H_2O and CO_2 in mafic magmas from Iacono-Marziano et al. (2012; Equations (1) and (2)). The parameters S_1 and S_2 in the solubility equations depend on the chemical make-up of the magma. We found that different mafic magma compositions did not significantly affect the outputs of our outgassing speciation model (Section 2.1); therefore, for the purposes of calculating melt solubility, we fixed the chemical make-up of the magma to the magma erupting at Mount Etna, Italy, reported by Iacono-Marziano et al. (2012). This reduced the complexity of the model without sacrificing any significant amount of accuracy.

Table 3 shows the chemical make-up of the magma at Mount Etna, and Table 4 shows several solubility constants from Iacono-Marziano et al. (2012). Together, these values define the solubility parameters S_1 and S_1:

$$S_1 = \ln\left(\frac{\mu_{magma}}{\mu_{CO_2} 10^6}\right) + \frac{C_{CO_2}P}{T} + B_{CO_2} + b_{CO_2}\left[\frac{\text{NBO}}{\text{O}}\right]$$
$$+ \left(\frac{x_{Al_2O_3}}{x_{CaO} + x_{K_2O} + x_{Na_2O}}\right)d_{Al_2O_3/(CaO + K_2O + Na_2O)}$$
$$+ (x_{FeO} + x_{MgO})d_{FeO + MgO} + (x_{Na_2O} + x_{K_2O})d_{Na_2O + K_2O}, \quad \text{(A1)}$$

Table 4
Solubility Constants

Constant	Value
C_{CO_2}	0.14
B_{CO_2}	−5.3
b_{CO_2}	15.8
B_{H_2O}	−2.95
b_{H_2O}	1.24
$d_{Al_2O_3/(CaO+K_2O+Na_2O)}$	3.8
$d_{FeO+MgO}$	−16.3
$d_{Na_2O+K_2O}$	20.1

Note. "Anhydrous" case from Iacono-Marziano et al. (2012).

$$S_2 = \ln\left(\frac{\mu_{magma}}{\mu_{H_2O} 10^2}\right) + \frac{C_{H_2O}P}{T} + B_{H_2O} + b_{H_2O}\left[\frac{\text{NBO}}{\text{O}}\right], \quad \text{(A2)}$$

Here T is magma temperature, P is the total pressure of degassing, and $\left[\frac{\text{NBO}}{\text{O}}\right]$ is the amount of nonbridging oxygen per oxygen in the melt.

A.2. Derivation of Equations (11) and (12)

The following is a derivation for the atom conservation equation for carbon used in our outgassing model (Equation (11)). The derivation for the atom conservation equation for hydrogen follows the exact same procedure, so we do not include it.

Consider some volume of magma with gas bubbles in it that contains a total number of moles γ_{tot}. The total moles is the sum of the moles of magma (γ_{magma}), and the moles of gas in bubbles suspended in that magma (γ_{gas}):

$$\gamma_{tot} = \gamma_{gas} + \gamma_{magma}. \quad \text{(A4)}$$

Within this same volume of magma, the total moles of carbon (γ_C^{tot}) is equal to the moles of carbon in the gas phase (γ_C^{gas}) and the moles of carbon dissolved in the magma (γ_C^{magma}) combined:

$$\gamma_C^{tot} = \gamma_C^{gas} + \gamma_C^{magma}. \quad \text{(A5)}$$

We assume that the only carbon-bearing molecule that can dissolve in the magma is CO_2; therefore, $\gamma_C^{magma} = \gamma_{CO_2}^{magma}$. Dividing by γ_{tot} and expanding gives

$$\frac{\gamma_C^{tot}}{\gamma_{tot}} = \frac{\gamma_{gas}}{\gamma_{tot}}\frac{\gamma_C^{gas}}{\gamma_{gas}} + \frac{\gamma_{magma}}{\gamma_{tot}}\frac{\gamma_{CO_2}^{magma}}{\gamma_{magma}}. \quad \text{(A6)}$$

We can replace $\frac{\gamma_{\text{magma}}}{\gamma_{\text{tot}}}$ with $1 - \frac{\gamma_{\text{gas}}}{\gamma_{\text{tot}}}$ using Equation (A4). This leaves us with

$$\frac{\gamma_C^{\text{tot}}}{\gamma_{\text{tot}}} = \frac{\gamma_{\text{gas}}}{\gamma_{\text{tot}}} \frac{\gamma_C^{\text{gas}}}{\gamma_{\text{gas}}} + \left(1 - \frac{\gamma_{\text{gas}}}{\gamma_{\text{tot}}}\right)\frac{\gamma_{CO_2}^{\text{magma}}}{\gamma_{\text{magma}}}. \quad (A7)$$

Here $\frac{\gamma_{CO_2}^{\text{magma}}}{\gamma_{\text{magma}}}$ is just x_{CO_2} (the mol fraction of CO_2 in the magma; see Table 1). Also, we assume that CO_2, CO, and CH_4 are the only carbon-bearing gas species, so $\gamma_C^{\text{gas}} = \gamma_{CO_2}^{\text{gas}} + \gamma_{CO}^{\text{gas}} + \gamma_{CH_4}^{\text{gas}}$. Making substitutions gives

$$\frac{\gamma_C^{\text{tot}}}{\gamma_{\text{tot}}} = \frac{\gamma_{\text{gas}}}{\gamma_{\text{tot}}} \frac{\gamma_{CO_2}^{\text{gas}} + \gamma_{CO}^{\text{gas}} + \gamma_{CH_4}^{\text{gas}}}{\gamma_{\text{gas}}} + \left(1 - \frac{\gamma_{\text{gas}}}{\gamma_{\text{tot}}}\right)x_{CO_2}. \quad (A8)$$

Assuming the ideal gas law, $\gamma_i^{\text{gas}}/\gamma_{\text{gas}} = P_i/P$. Also, to make the equation more manageable, we substitute $\alpha_{\text{gas}} = \frac{\gamma_{\text{gas}}}{\gamma_{\text{tot}}}$, which is the total mols in the gas phase divided by the moles in the gas phase and magma combined:

$$\frac{\gamma_C^{\text{tot}}}{\gamma_{\text{tot}}} = \frac{P_{CO_2} + P_{CO} + P_{CH_4}}{P}\alpha_{\text{gas}} + (1 - \alpha_{\text{gas}})x_{CO_2}. \quad (A9)$$

Magma sometimes freezes deep in the Earth as a glass before it releases any volatiles. Measurements of volatiles like CO_2 in such glasses are reported in terms of mass fractions (Wallace et al. 2015). To stay consistent with these unit conventions, we indicate the total carbon in un-degassed magma as a mass fraction of CO_2 (m_{CO2}^{tot}). We can convert the mass fraction to a mole fraction using Equation (3):

$$\frac{m_{CO2}^{\text{tot}}\mu_{\text{magma}}}{\mu_{CO_2}} = x_{CO2}^{\text{tot}} = \frac{\gamma_{CO_2}^{\text{tot}}}{\gamma_{\text{tot}}} = \frac{\gamma_C^{\text{tot}}}{\gamma_{\text{tot}}}. \quad (A10)$$

Substituting Equation (A10) into Equation (A9) gives

$$\frac{m_{CO_2}^{\text{tot}}\mu_{\text{magma}}}{\mu_{CO_2}} = \frac{P_{CO_2} + P_{CO} + P_{CH_4}}{P}\alpha_{\text{gas}}$$
$$+ (1 - \alpha_{\text{gas}})x_{CO_2}. \quad (A11)$$

Equation (A11) is identical to Equation (11).

A.3. Graphite Saturation and the Solubility of CO, CH₄, and H₂

Several studies have shown that degassing can be affected by graphite saturation of magma (Hirschmann & Withers 2008) or by the solubility of CO, CH₄, and H₂ in magma (Hirschmann et al. 2012; Ardia et al. 2013; Wetzel et al. 2013). Our model for outgassing speciation used throughout the main text does not account for these complications. Here we show that our assumption is valid because it does not significantly change our results.

Consider the following equilibrium:

$$C + O_2 \leftrightarrow CO_2, \quad (A12)$$

$$K_9 = \frac{f_{CO_2}}{a_C f_{O_2}} \approx \frac{P_{CO_2}}{a_C f_{O_2}}. \quad (A13)$$

Here K_9 is the equilibrium constant given by $\exp(47457/T + 0.136)$, and a_C is the activity of carbon. To incorporate graphite saturation into our model, we first calculate outgassing speciation using the model described in the main text (Section 2.1). Next, we check for graphite saturate by calculating

the activity of carbon using Equation (A13). If $a_C < 1$, then we assume the melt is not graphite saturated and that the calculation is valid. If $a_C > 1$, then we assume graphite is saturated and recalculate outgassing speciation by replacing the carbon conservation equation (Equation (11)), with the graphite saturation equation with $a_C = 1$ (Equations (A13)). Here we are considering graphite saturation in the magma just before degassing occurs. Our treatment is different from, for example, the methods of Ortenzi et al. (2020) because they are accounting for graphite saturation much deeper in a planet during partial melting of the mantle.

Figure 10 is identical to Figure 3, except Figure 10 accounts for graphite saturation. Graphite saturation appears to have a small effect on the results; therefore, it is justified to ignore it.

To incorporate the solubility of H₂, CH₄, and CO into our model, we add the following solubility relationships to or system of original outgassing equations (Section 2.1):

$$\exp(-11.403 - 0.000076P) = K_5 = \frac{x_{H_2}}{f_{H_2}} \approx \frac{x_{H_2}}{P_{H_2}}, \quad (A14)$$

$$\exp(-7.63 - 0.000193P) = K_6 = \frac{x_{CH_4}}{f_{CH_4}} \approx \frac{x_{CH_4}}{P_{CH_4}}, \quad (A15)$$

$$\exp(-41.02 - 0.00056P) = K_7 = \frac{x_{Fe(CO)_5}}{a_{Fe} f_{CO}^5} \approx \frac{x_{Fe(CO)_5}}{a_{Fe} P_{CO}^5}. \quad (A16)$$

Here pressure-dependent equilibrium constants K_5, K_6, and K_7 are from Hirschmann et al. (2012), Ardia et al. (2013), and Wetzel et al. (2013), respectively. For Equation (A16), we take the activity of iron to be $a_{Fe} = 0.6$, based on the experiments in Wetzel et al. (2013). Also, we only include the Equation (A16) when $f_{O_2} <$ IW-0.55 (IW is the iron-wustite mineral buffer) because Wetzel et al. (2013) only observed CO dissolved in magma for these low oxygen fugacities.

We also alter the carbon and hydrogen atom conservation equations to accommodate for new molecules in the melt.

$$\frac{m_{CO_2}^{\text{tot}}\mu_{\text{magma}}}{\mu_{CO_2}} = \frac{P_{CO_2} + P_{CO} + P_{CH_4}}{P}\alpha_{\text{gas}}$$
$$+ (1 - \alpha_{\text{gas}})(x_{CO_2} + x_{CO} + x_{CH_4}), \quad (A17)$$

$$\frac{m_{H_2O}^{\text{tot}}\mu_{\text{magma}}}{\mu_{H_2O}} = \frac{P_{H_2O} + P_{H_2} + 2P_{CH_4}}{P}\alpha_{\text{gas}}$$
$$+ (1 - \alpha_{\text{gas}})(x_{H_2O} + x_{H_2} + 2x_{CH_4}). \quad (A18)$$

Here x_i is the mol fraction of species i in the melt.

Figure 11 is identical to Figure 3, except Figure 11 accounts for H₂, CH₄, and CO solubility in magma. The solubility of these three molecules has a small effect on the results; therefore they can be ignored.

A.4. Closed System Cooling and Chemical Kinetics

Our model for volcanic outgassing is a thermodynamic equilibrium model. We assume that during magma eruptions, gas bubbles chemically and thermally equilibrate with magma, and then they are released to the atmosphere unaltered (Figure 1). This does not exactly reflect real degassing.

In reality, the chemical composition of gas bubbles changes as bubbles leave the magma and enter the atmosphere
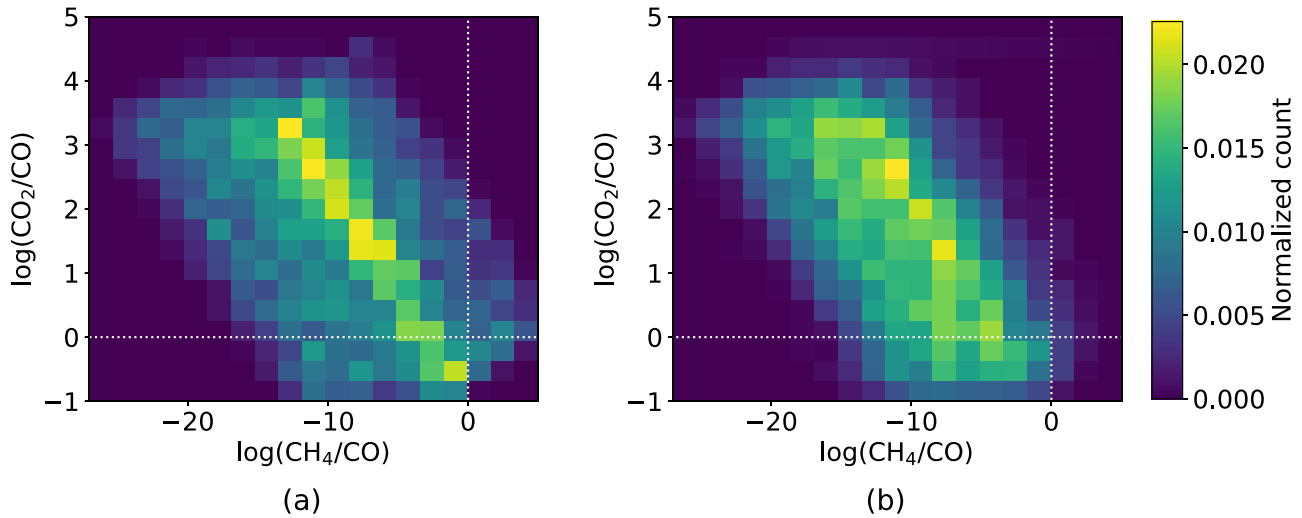
Figure 10. Identical to Figure 3, except here we account for graphite saturation in the melt. As in Figure 3, (a) is for ocean worlds and (b) is for Earth-like worlds. Graphite saturation has a small effect on the results.
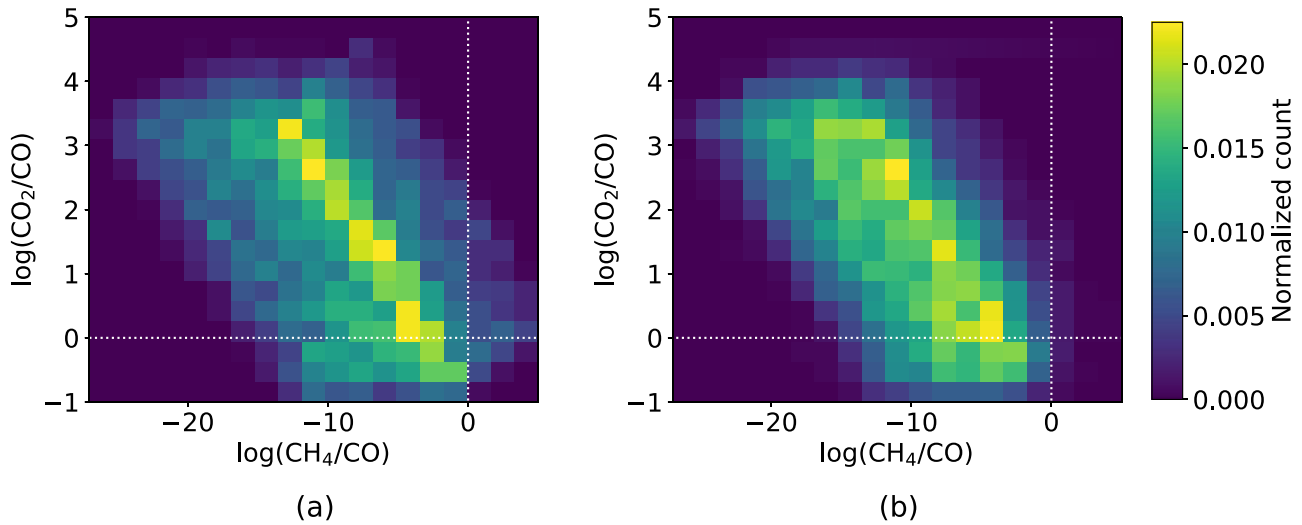

Figure 11. Identical to Figure 3, except here we account for the solubility of H_2, CH_4, and CO in the melt. As in Figure 3, (a) is for ocean worlds and (b) is for Earth-like worlds. H_2, CH_4, and CO solubility have a small effect on the results.

(Moussallam et al. 2019; Kadoya et al. 2020). As a bubble leaves magma, it cools down and new chemical equilibria are preferred. When a gas bubble first begins cooling, it is still very hot, so chemical reactions keep the bubble near chemical equilibrium. Once the bubble is cold enough, chemical reactions slow, and ultimately cease, quenching or freezing the chemical composition of the gas bubble. Therefore, the cooling process alters the chemistry of the gas.

Gas re-equilibration to lower temperatures explains the observed chemistry of volcanic gases globally (Moussallam et al. 2019), and Oppenheimer et al. (2018) provides a specific example of this phenomenon at in the Kilauea volcano in Hawaii. During eruptions at Kilauea, gas bubbles in the magma would rise to the surface. As the bubbles rose in the magma, they adiabatically expanded, which cooled the gas below the temperature of the magma. Chemical reactions during adiabatic expansion changed the chemical make-up of the bubble.

For the purposes of understanding potential CH_4 biosignature false positives from volcanoes, we need to know if bubble cooling might generate a substantial amount of CH_4. Here we first consider the kinetics of methane generation and show that reactions are likely too slow to generate substantial CH_4 during gas cooling. Next, we show that our Monte Carlo simulation results (Figure 4) remain qualitatively unchanged, even if our kinetics calculations are wrong, and CH_4 can be generated during gas cooling.

CO or CO_2 is converted to CH_4 through either of the net reactions (Schaefer & Fegley 2010):

$$CO + 3H_2 \leftrightarrow CH_4 + H_2O, \qquad (A19)$$

$$CO_2 + 4H_2 \leftrightarrow CH_4 + 2H_2O. \qquad (A20)$$
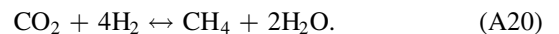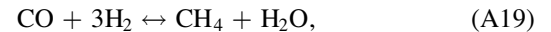
The rate-limiting step to either CO or CO_2 conversion to CH_4 is debated in the literature (Zahnle & Marley 2014), but the following are two solid candidates and their corresponding rate constants:

$$H_2 + H_2CO \rightarrow CH_3 + OH, \qquad (A21)$$
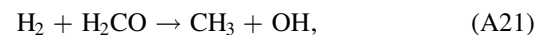
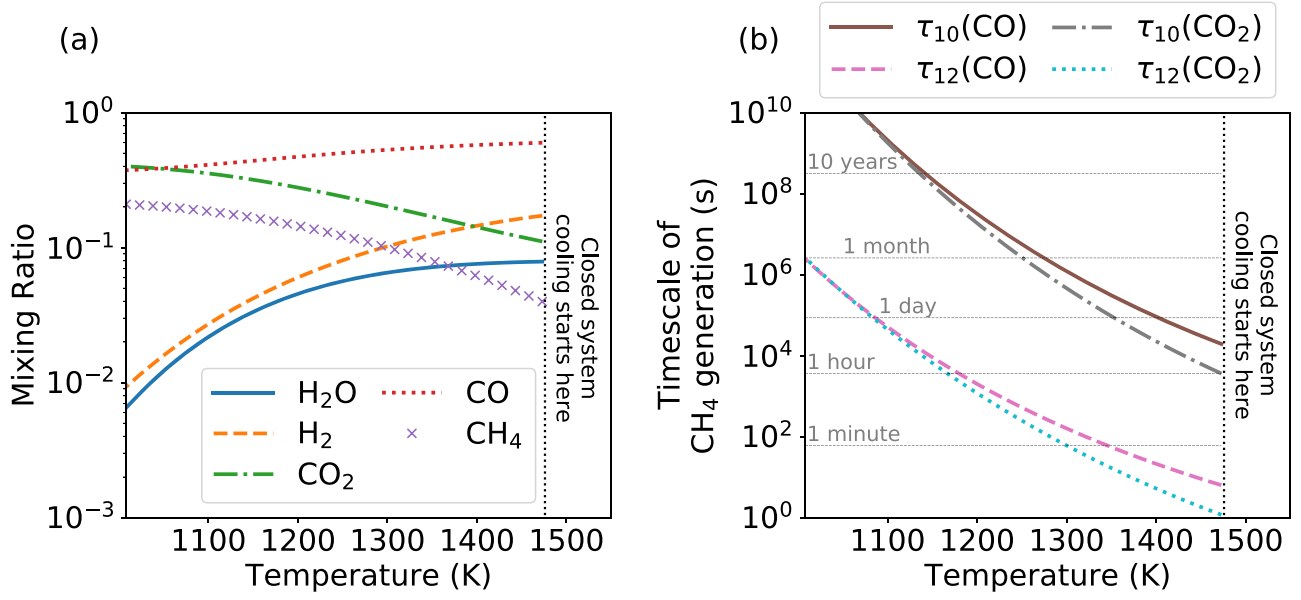$$k_{10} = 2.3 \times 10^{-10} \exp(-36200/T), \qquad (A22)$$

Figure 12. (a) Equilibrium composition as a function of temperature for a submarine volcanic gas that is cooled as a closed system and (b) timescales of CH_4 formation during closed system cooling. Timescales of volcanic gas cooling are not shown or calculated.
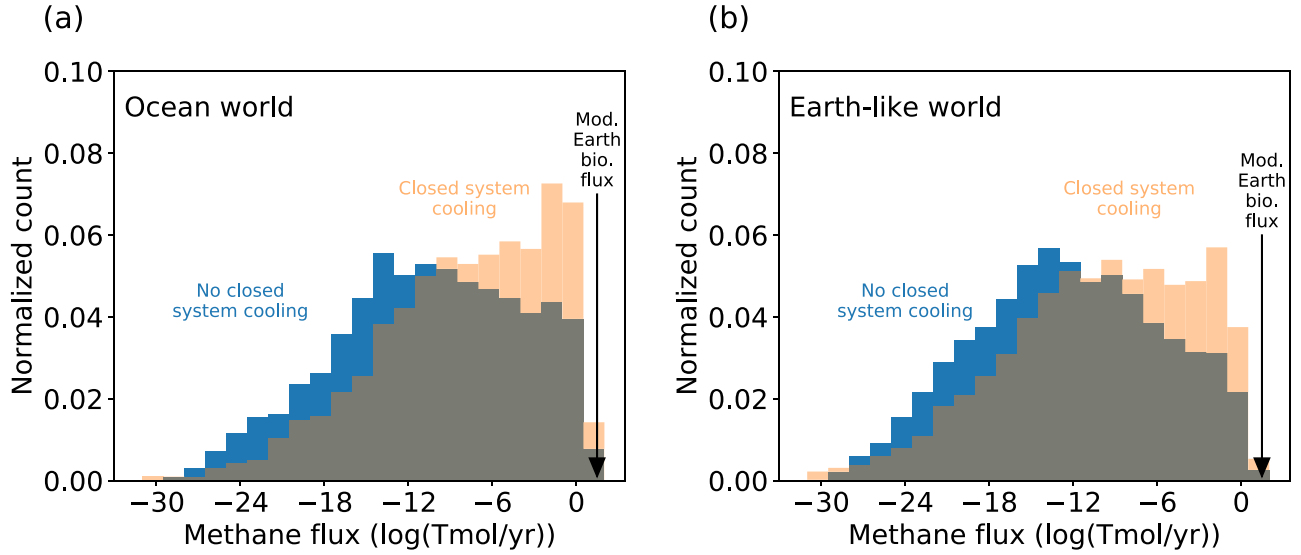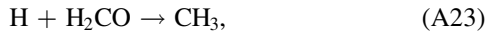

Figure 13. The blue histograms in (a) and (b) are identical to Figures 4(c) and (d), and orange histograms are identical Monte Carlo simulations, except they account for the closed system cooling of volcanic gases to equilibrium temperatures observed on Earth (800 to 1500 K). To calculate CH_4 fluxes, we used modern Earth's magma production rate.

$$H + H_2CO \rightarrow CH_3, \tag{A23}$$

$$k_{12} = 4.0 \times 10^{-11} \exp(-2068/T). \tag{A24}$$

Here k_{10} and k_{12} are rate constants ($cm^3\ s^{-1}$). The lifetime of CO or CO_2 conversion to CH_4 is thus one of the following:

$$\tau_{10}(CO) = \frac{N_{CO}}{k_{10}N_{H_2}N_{H_2CO}}, \tag{A25}$$

$$\tau_{12}(CO) = \frac{N_{CO}}{k_{12}N_H N_{H_2CO}}, \tag{A26}$$

$$\tau_{10}(CO_2) = \frac{N_{CO_2}}{k_{10}N_{H_2}N_{H_2CO}}, \tag{A27}$$

$$\tau_{12}(CO_2) = \frac{N_{CO_2}}{k_{12}N_H N_{H_2CO}}. \tag{A28}$$

Here τ is the chemical lifetime in seconds, and N_i is the number density of species i in molecules cm^{-3}.

Figure 12 shows timescales of CH_4 generation (Equations (A25)–(A28)) during the closed system cooling of submarine volcanic gas. To determine gas chemistry just before a bubble is released from magma, we use our speciation model (Section 2.1). At 1473 K, we calculate gas speciation assuming $P = 400\ \text{bar}$, $f_{O_2} = \text{FMQ-4}$, $m_{CO_2}^{tot} = 0.1\%$, and $m_{H_2O}^{tot} = 0.5\%$. We then calculate new chemical equilibrium as the gas cools, assuming it is a closed system (i.e., we assume the gas is

thermally and chemically decoupled from the magma; Figure 12(a)). Figure 12(b) shows the corresponding timescale of CH_4 generation (Equations (A25)–(A28)) at each temperature.

The quench temperature (i.e., the temperature where outgassing chemistry is frozen-in due to slow kinetics) of CH_4 depends on the cooling timescale of volcanic gases (not shown in Figure 12). CH_4 should quench where the cooling timescale is about the same as the timescale of CH_4 generation. After gases are released from a submarine volcano, we suspect they cool from magma temperatures to ocean temperatures on the order of seconds. If this is the case, then the CH_4 quench temperature is probably >1400 K. This would result in a negligible increase in the CH_4 content of the gas (Figure 12(a)).

Suppose that the CH_4 quench temperature was instead 1000 K. In this case, the CH_4 content of the gas would be increased by about a factor of five (Figure 12(a)). There are two ways that a ∼1000 K CH_4 quench is possible. First, gas cooling could occur on timescales of months rather than seconds. According to Figure 12(b), month-long gas cooling should quench CH_4 by 1000 K. Second, catalysts could dramatically speed up the reactions creating CH_4, which might allow for quench temperatures near 1000 K for even gas cooling timescales of seconds. In the following two paragraphs, we show that either of these scenarios would not significantly change our results.

To demonstrate that re-equilibration of gases to feasible lower temperatures does not change our conclusions, assuming low CH_4 quench temperatures can be achieved, we perform another Monte Carlo simulation identical to the one described in Section 2.2, except we account for closed system cooling of volcanic gases. In the Monte Carlo simulation, we first calculate gas composition using our outgassing model (Section 2.1); then we re-equilibrate this gas mixture to the uniformly sampled gas equilibrium temperature between 800 and 1500 K. This range of gas equilibrium temperatures is the range observed in Earth's volcanic gases (Moussallam et al. 2019). In cases where the randomly drawn gas equilibrium temperature is higher than the magma temperature, we assume no closed system cooling occurs.

Figure 13 is identical to Figures 4(c) and (d), except Figure 13 accounts for closed system cooling of gases. Closed system cooling allows more CH_4 production on average, but still only 0.3% and 0.1% of calculations for ocean worlds or earth-like worlds, respectively, produce more than 10 Tmol $CH_4 \, yr^{-1}$. The probability of volcanic CH_4 fluxes being comparable to modern Earth's biological flux (30 Tmol yr^{-1}) is still low.

In summary, changes in gas chemistry during cooling might cause our speciation model to under-predict the CH_4 produced by an amount that does not change our conclusions significantly. Further consideration of the kinetics of CH_4 generation in volcanic gases is beyond the scope of this paper.

Appendix B
Photochemical Model Boundary Conditions

Table 5 shows boundary conditions used for the *Atmos* photochemical model. We used the same H_2O and temperature profile as Kharecha et al. (2005) for all simulations. The version of Atmos that we used has updated rate constants and H_2O cross sections following Ranjan et al. (2020).

Every simulation for planets orbiting the Sun uses a solar spectrum at 2.7 Ga, calculated via the methods described in

Table 5
Boundary Conditions for Photochemical Modeling

Chemical species	Deposition velocity (cm s^{-1})	Mixing ratio	Flux (molecules cm^{-2} s^{-1})
O	1	…	…
O_2	1.4×10^{-4}	…	…
H_2O	0	…	…
H	1	…	…
OH	1	…	…
HO_2	1	…	…
H_2O_2	2×10^{-1}	…	…
H_2	0	…	$5.9F_{CH_4}$
CO	1×10^{-8}	…	$1.7F_{CH_4}$
HCO	1	…	…
H_2CO	2×10^{-1}	…	…
CH_4	0	…	variable
CH_3	1	…	…
C_2H_6	0	…	…
NO	3×10^{-4}	…	…
NO_2	3×10^{-3}	…	…
HNO	1	…	…
O_3	7×10^{-2}	…	…
HNO_3	2×10^{-1}	…	…
H_2S	2×10^{-2}	…	$0.1F_{CH_4}$
SO_3	0	…	…
S_2	0	…	…
HSO	1	…	…
H_2SO_4	1	…	…
SO_2	1	…	$0.1F_{CH_4}$
SO	0	…	…
SO_4 aerosol	1×10^{-2}	…	…
S_8 aerosol	1×10^{-2}	…	…
Hydrocarbon aerosol	1×10^{-2}	…	…
CO_2	…	Variable	…
N_2	…	0.8	…

Note. Species included in the photochemical scheme with a deposition velocity and flux of 0 include N, C_3H_2, C_3H_3, CH_3C_2H, CH_2CCH_2, C_3H_5, C_2H_5CHO, C_3H_6, C_3H_7, C_3H_8, C_2H_4OH, C_2H_2OH, C_2H_5, C_2H_4, CH, CH_3O_2, CH_3O, CH_2CO, CH_3CO, CH_3CHO, C_2H_2, $(CH_2)_3$, C_2H, C_2, C_2H_3, HCS, CS_2, CS, OCS, S, and HS. Here deposition velocities follow those used by Schwieterman et al. (2019).

Claire et al. (2012), although our results are not sensitive to the age of the Sun. For planets orbiting an M8V star, we use estimates of TRAPPIST-1's spectrum derived by Lincowski et al. (2018), scaled so that the solar constant of the planet is 0.822 relative to modern Earth's. We use this solar constant because it places the simulated planet at the same relative distance from the inner edge of the habitable zone as Earth today (Kopparapu et al. 2013).

All of our models include the modern production rate of NO from lightning.

ORCID iDs

Nicholas Wogan https://orcid.org/0000-0002-0413-3308

References

Adam, P. S., Borrel, G., & Gribaldo, S. 2018, PNAS, 115, E1166
Anderson, K. R., & Poland, M. P. 2017, NatGe, 10, 704
Ardia, P., Hirschmann, M. M., Withers, A., & Stanley, B. 2013, GeCoA, 114, 52

Armstrong, K., Frost, D. J., McCammon, C. A., Rubie, D. C., & Ballaran, T. B. 2019, Sci, 365, 903

Barstow, J. K., & Irwin, P. G. 2016, MNRAS: Letters, 461, L92

Benner, S. A., Bell, E. A., Biondi, E., et al. 2019, ChemSystemsChem, 2, e1900035

Burcat, A., & Ruscic, B. 2005, Third Millenium Ideal Gas and Condensed Phase Thermochemical Database for Combustion (with update from active thermochemical tables) Tech Rep. ANL-05/20 (Argonne National Lab, Argonne, IL), doi:10.2172/925269

Catling, D. C., & Kasting, J. F. 2017, Atmospheric Evolution on Inhabited and Lifeless Worlds (Cambridge: Cambridge Univ. Press)

Catling, D. C., & Zahnle, K. J. 2020, SciA, 6, eaax1420

Claire, M. W., Catling, D. C., & Zahnle, K. J. 2006, Geobiology, 4, 239

Claire, M. W., Sheets, J., Cohen, M., et al. 2012, ApJ, 757, 95

Crisp, J. A. 1984, JVGR, 20, 177

Domagal-Goldman, S. D., Segura, A., Claire, M. W., Robinson, T. D., & Meadows, V. S. 2014, ApJ, 792, 90

Doyle, A. E., Young, E. D., Klein, B., Zuckerman, B., & Schlichting, H. E. 2019, Sci, 366, 356

Fauchez, T. J., Turbet, M., Villanueva, G. L., et al. 2019, ApJ, 887, 194

Fischer, W. W., Hemp, J., & Johnson, J. E. 2016, AREPS, 44, 647

French, B. M. 1966, RvGeo, 4, 223

Gaillard, F., & Scaillet, B. 2014, E&PSL, 403, 307

Gilbert, W. 1986, Natur, 319, 618

Gonnermann, H. M., & Manga, M. 2013, in Modeling Volcanic Processes: The Physics and Mathematics of Volcanism, ed. R. M. C. Lopes, S. A. Fagents, & T. K. P. Gregg (Cambridge: Cambridge Univ. Press), 55

Grenfell, J. L., Gebauer, S., Paris, P. v., Godolt, M., & Rauer, H. 2014, P&SS, 98, 66

Grenfell, J. L., Grießmeier, J.-M., Patzer, B., et al. 2007, AsBio, 7, 208

Guzmán-Marmolejo, A., Segura, A., & Escobar-Briones, E. 2013, AsBio, 13, 550

Harman, C. E., Schwieterman, E. W., Schottelkotte, J. C., & Kasting, J. F. 2015, ApJ, 812, 137

Hauglustaine, D., Heinze, C., Holland, E., et al. 2007, in Climate Change 2007: The Physical Science Basis. Contribution of Working Group I to the Fourth Assessment Report of the Intergovernmental Panel on Climate Change, ed. S. Solomon et al. (Cambridge: Cambridge Univ. Press)

Hirschmann, M. M., Withers, A., Ardia, P., & Foley, N. 2012, E&PSL, 345, 38

Hirschmann, M. M., & Withers, A. C. 2008, E&PSL, 270, 147

Holland, H. D. 1984, The Chemical Evolution of the Atmosphere and Oceans (Princeton, NJ: Princeton Univ. Press)

Huppert, H. E., Sparks, R. S. J., Turner, J. S., & Arndt, N. T. 1984, Natur, 309, 19

Iacono-Marziano, G., Morizet, Y., le Trong, E., & Gaillard, F. 2012, GeCoA, 97, 1

Joyce, G. F., & Szostak, J. W. 2018, Cold Spring Harbor Perspectives in Biology, 10, a034801

Kadoya, S., Catling, D. C., Nicklas, R. W., Puchtel, I. S., & Anbar, A. D. 2020, Geochemical Perspectives Letters, 13, 25

Kasting, J. F., & Brown, L. L. 1998, in The Molecular Origins of Life, ed. A. Brack (Cambridge: Cambridge Univ. Press), 35

Kasting, J. F., & Catling, D. 2003, ARA&A, 41, 429

Kharecha, P., Kasting, J., & Siefert, J. 2005, Geobiology, 3, 53

Kopparapu, R. K., Ramirez, R., Kasting, J. F., et al. 2013, ApJ, 765, 131

Krissansen-Totton, J., Garland, R., Irwin, P., & Catling, D. C. 2018a, AJ, 156, 114

Krissansen-Totton, J., Olson, S., & Catling, D. C. 2018b, SciA, 4, eaao5747

le Voyer, M., Hauri, E. H., Cottrell, E., et al. 2019, GGG, 20, 1387

Lehmer, O. R., Catling, D. C., Parenteau, M. N., & Hoehler, T. M. 2018, ApJ, 859, 171

Li, Z.-X. A., & Lee, C.-T. A. 2004, E&PSL, 228, 483

Liggins, P., Shorttle, O., & Rimmer, P. B. 2020, E&PSL, 550, 116546

Lincowski, A. P., Meadows, V. S., Crisp, D., et al. 2018, ApJ, 867, 76

Luger, R., & Barnes, R. 2015, AsBio, 15, 119

Lustig-Yaeger, J., Meadows, V. S., & Lincowski, A. P. 2019, AJ, 158, 27

Lyons, T. W., Reinhard, C. T., & Planavsky, N. J. 2014, Natur, 506, 307

Marchi, S., Bottke, W., Elkins-Tanton, L., et al. 2014, Natur, 511, 578

McKenzie, D. 2020, JPet, egaa061

Meadows, V. S. 2017, AsBio, 17, 1022

Meadows, V. S., Reinhard, C. T., Arney, G. N., et al. 2018, AsBio, 18, 630

Miller, S. L., & Urey, H. C. 1959, Sci, 130, 245

Moussallam, Y., Oppenheimer, C., & Scaillet, B. 2019, E&PSL, 520, 260

O'Neill, H. S. 1987, AmMin, 72, 67, http://www.minsocam.org/ammin/AM72/AM72_67.pdf

Oppenheimer, C., Scaillet, B., Woods, A., et al. 2018, NatGe, 11, 678

Ortenzi, G., Noack, L., Sohl, F., et al. 2020, NatSR, 10, 10907

Pavlov, A. A., Brown, L. L., & Kasting, J. F. 2001, JGR, 106, 23267

Ranjan, S., Schwieterman, E. W., Harman, C., et al. 2020, ApJ, 896, 148

Reeves, E. P., & Fiebig, J. 2020, Elements: An International Magazine of Mineralogy, Geochemistry, and Petrology, 16, 25

Ritson, D. J., Battilocchio, C., Ley, S. V., & Sutherland, J. D. 2018, NatCo, 9, 1

Rugheimer, S., & Kaltenegger, L. 2018, ApJ, 854, 19

Rugheimer, S., Kaltenegger, L., Segura, A., Linsky, J., & Mohanty, S. 2015, ApJ, 809, 57

Sasselov, D. D., Grotzinger, J. P., & Sutherland, J. D. 2020, SciA, 6, eaax3419

Sauterey, B., Charnay, B., Affholder, A., Mazevet, S., & Ferrière, R. 2020, NatCo, 11, 1

Schaefer, L., & Fegley, B., Jr 2010, Icar, 208, 438

Scheidegger, K. 1973, JGR, 78, 3340

Schindler, T. L., & Kasting, J. F. 2000, Icar, 145, 262

Schwieterman, E. W., Reinhard, C. T., Olson, S. L., et al. 2019, ApJ, 874, 9

Segura, A., Kasting, J. F., Meadows, V., et al. 2005, AsBio, 5, 706

Sholes, S. F., Krissansen-Totton, J., & Catling, D. C. 2019, AsBio, 19, 655

Sleep, N. H., & Zahnle, K. 2001, JGR, 106, 1373

Smith, M. L., Claire, M. W., Catling, D. C., & Zahnle, K. J. 2014, Icar, 231, 51

Stamper, C., Melekhova, E., Blundy, J., et al. 2014, CoMP, 167, 954

Strobel, D. F., Atreya, S. K., Bézard, B., et al. 2009, in Titan from Cassini-Huygens, ed. R. H. Brown et al. (Berlin: Springer), 235

Sutherland, J. D. 2016, Angewandte Chemie International Edition, 55, 104

Symonds, R. B., Rose, W. I., Bluth, G. J. S., & Gerlach, T. M. 1994, in Volatiles in Magma, Reviews in Mineralogy, Vol. 30, ed. M. R. Carrol & J. R. Halloway (Chantilly, VA: Mineralogical Society of America), 1

Tian, F., France, K., Linsky, J. L., Mauas, P. J., & Vieytes, M. C. 2014, E&PSL, 385, 22

Tian, F., Kasting, J., & Zahnle, K. 2011, E&PSL, 308, 417

Tutolo, B. M., Seyfried, W. E., & Tosca, N. J. 2020, PNAS, 117, 14756

Wallace, P. J. 2005, JVGR, 140, 217

Wallace, P. J., Plank, T., Edmonds, M., & Hauri, E. H. 2015, Volatiles in Magmas (Amsterdam: Elsevier), 163, doi:10.1016/B978-0-12-385938-9.00007-9

Wetzel, D. T., Rutherford, M. J., Jacobsen, S. D., Hauri, E. H., & Saal, A. E. 2013, PNAS, 110, 8010

Wones, D. R., & Gilbert, M. C. 1969, AmJS, 267, 480

Wordsworth, R., & Pierrehumbert, R. 2014, ApJL, 785, L20

Wunderlich, F., Scheucher, M., Godolt, M., et al. 2020, ApJ, 901, 126

Zahnle, K., Claire, M., & Catling, D. 2006, Geobiology, 4, 271

Zahnle, K., Haberle, R. M., Catling, D. C., & Kasting, J. F. 2008, JGRE, 113, E11004

Zahnle, K. J. 1986, JGR, 91, 2819

Zahnle, K. J., Lupu, R., Catling, D. C., & Wogan, N. 2020, PSJ, 1, 11

Zahnle, K. J., & Marley, M. S. 2014, ApJ, 797, 41